Istituto Universitario di Studi Superiori di Pavia

Development of Simplified Tools for the Design and Assessment of Eccentrically Braced Steel Frames

An Individual Study Submitted in Partial Fulfilment of the Requirements
for the Degree of Doctor of Philosophy in

EARTHQUAKE ENGINEERING AND ENGINEERING SEISMOLOGY

Obtained in the framework of the Doctoral Programme in
Understanding and Managing Extremes

by

Gerard J. O'Reilly

December, 2015

IUSS

Scuola Universitaria Superiore Pavia

Istituto Universitario di Studi Superiori di Pavia

Development of Simplified Tools for the Design and Assessment of Eccentrically Braced Steel Frames

An Individual Study Submitted in Partial Fulfilment of the Requirements
for the Degree of Doctor of Philosophy in

EARTHQUAKE ENGINEERING AND
ENGINEERING SEISMOLOGY

Obtained in the framework of the Doctoral Programme in
Understanding and Managing Extremes

by

Gerard J. O'Reilly

Supervisors: Prof. Timothy J. Sullivan

December, 2015

ABSTRACT

Eccentrically braced frames (EBFs) represent an attractive lateral load resisting steel system to be used in areas of high seismicity. The focus of this report is to provide a set of simplified tools for both the design and assessment of EBF structures. Regarding the design of EBF structures, a recently proposed direct displacement-based design (DDBD) procedure for EBFs is described and further developed in this report through the calibration of a spectral displacement reduction factors that relate the displacement of an inelastically responding structure to that of the equivalent linear representation used in the DDBD of EBFs. Such an expression is calibrated as part of this study using an experimentally validated numerical model. The DDBD guidelines are applied to EBF systems from 1 to 15 storeys in height and their performance is verified via nonlinear response history analyses using two different sets of design spectrum compatible ground motions. The results of the study indicate the robustness of the proposed DDBD method in limiting the interstorey drifts to design limits for a variety of EBF systems with short links, thus demonstrating that the proposed DDBD method is an effective tool for seismic design of EBFs. In addition to the proposal of DDBD guidelines for the design of EBFs, a series of eccentrically braced frames are also designed and subjected to nonlinear analyses to highlight ambiguities and differences in current seismic design provisions for EBF structures to provide further motivation for implementing better guidance in checking local displacement demands and further support a move towards a displacement-based design approach.

In order to assess the likely damage for a given intensity of ground shaking, fragility functions can be used to identify the probability of exceeding a certain damage limit-state, given a certain response of a structure. This paper also develops a set of fragility functions for EBF structures, considering that damage can be directly linked to the interstorey drift demand at each storey. This is done by performing a Monte Carlo Simulation of an analytical expression for the drift capacity of an EBF, where each term of the expression relies on either experimental testing results or mechanics-based reasoning. The analysis provides a set of fragility functions that can be used for three damage limit-states: concrete slab repair, damage requiring heat straightening of the link and damage requiring link replacement. Depending on the level of detail known about the structure, in terms of its link section size, link length and storey number within a structure, the resulting fragility function can be refined and its associated epistemic uncertainty reduced. This is done by using an analytical expression to estimate the median

value of interstorey drift, which can be used in conjunction with an informed assumption of dispersion, or alternatively by using a MATLAB-based tool that calculates the median and dispersion for each damage limit-state for a given set of user specified inputs about the EBF. However, a set of general fragility functions is also provided to enable quick assessment of EBF structures at a regional scale.

TABLE OF CONTENTS

LIST OF FIGURES

LIST OF TABLES

1. INTRODUCTION

1.1 OVERVIEW

Eccentrically braced frames (EBFs) represent an attractive lateral load resisting steel system to be used in areas of high seismicity. A recently proposed direct displacement-based design (DDBD) procedure for EBFs is described and developed further through the use of more refined analysis using a newly calibrated numerical model for EBF links. The DDBD guidelines are applied to EBF systems from 1 to 15 storeys in height and their performance is verified via nonlinear dynamic analyses using two different sets of design spectrum compatible ground motions. In addition to the design of EBF structures, in order to assess the likely damage for a given intensity of ground shaking, fragility functions can be used to identify the probability of exceeding a certain damage limit-state, given a certain response of a structure. This report also looks at developing a set of fragility functions for EBF structures, considering that damage can be directly linked to the interstorey drift demand.

1.2 LAYOUT OF THE REPORT

The research contained within this research report has been peer-reviewed and published in two different journal articles. As such, this report will report the two as-accepted journal articles and provide a more general set of conclusions from the research in the final chapter of this report. Chapter 2 discusses the development of the DDBD of EBFs, where by a new numerical model for the nonlinear analysis of EBF frames is developed and validated using existing experimental results. Additional tools to aid the DDBD of EBFs are also proposed and discussed in Chapter 2. Regarding the damage assessment of EBF structures, Chapter 3 outlines the development of a set of fragility functions that can be used to identify different link damage states as a function of interstorey drift. Various sets of fragility functions are proposed depending on the level of detail known about the structure and an example implementation of each of these fragility function sets is also provided. Chapter 4 then concludes the research and highlights the principal findings from this research report.

2. DIRECT DISPLACEMENT-BASED DESIGN OF ECCENTRICALLY BRACED STEEL FRAMES

This chapter is based on work published in O'Reilly and Sullivan [2015], available at:

O'Reilly, G. J., Sullivan, T. J. [2015] "Direct Displacement-Based Seismic Design of Eccentrically Braced Steel Frames," *Journal of Earthquake Engineering*, Taylor & Francis, pp. 1–36.

2.1 INTRODUCTION

Investigations into the seismic behaviour of eccentrically braced steel frames (EBFs) appear to have originated in Japan during the 1970's, where Tanabashi *et al.* [1974] performed a series of static tests on vertical Y-link configurations to examine the hysteretic properties of this eccentric configuration. Extensive experimental investigations into the behaviour of EBF structures using horizontal links, such as that shown in Figure 2.1, were conducted at the University of California at Berkeley in the late 1970's/early 1980's [Engelhardt and Popov, 1989b; Hjelmstad and Popov, 1983; Kasai and Popov, 1986; Popov and Malley, 1983; Roeder and Popov, 1977], where numerous experiments were performed to determine the behaviour of these links and the influence of stiffener detailing on their performance, and also more recently at the University of Texas during the 2000's [Arce, 2002; Galvez, 2004; Okazaki and Engelhardt, 2007; Ryu, 2005]. These tests formed the basis for the development of the EBF system, as these experimental campaigns demonstrated the stable hysteretic behaviour of ductile links. One aspect of the EBF that makes it particularly desirable as a ductile lateral load resisting system is that it possesses an initial stiffness similar to a concentrically braced frame, which is generally seen to be beneficial in terms of limiting lateral displacements and storey drift, but also having the energy dissipation capacity of a moment-resisting frame, where the stable hysteretic response of the links dissipate large amounts of energy in comparison to a similar concentrically braced frame configuration.
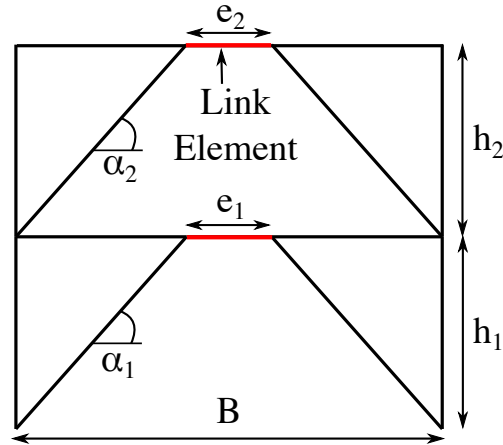
Figure 2.1: Typical layout of an EBF.

In comparison to other steel structures, such as moment-resisting frames and concentrically braced frames, reconnaissance information for EBFs is not widely available. However, a series of post-earthquake investigations have been conducted for a number of EBF structures subjected to the 2010 and 2011 Canterbury earthquakes in New Zealand, which reported on damage to both medium and high-rise EBF building structures, as well as parking garages, subject to the two different earthquakes. Bruneau *et al.* [2010] notes that recently constructed buildings in the downtown Christchurch area, such as the 22 storey Pacific Residential Tower, relied on EBFs as the lateral load resisting system. In general, these structures were reported as having performed very well with only minor flaking of the link element paint being reported, which led to these structures being green-tagged following the earthquake. Clifton *et al.* [2011] noted that estimates of peak shear strain demand were of the order of 0.03-0.04 rad in one structure, which is well below the NZS3404 [NZS 3404, 2007] limit of 0.08 rad if shear strain is taken to be equal to the link chord rotation, although this structure was noted to have been designed for a lower target ductility due to its height and plan dimensions [Bruneau *et al.*, 2010]. This was again the case for the 2011 event, as reported by [Bruneau *et al.*, 2011], which is an interesting point as both events were generally stronger than the design demand level specified by NZS3404.

Design codes such as Eurocode 8 [EN 1998-1:2004, 2004], New Zealand's NZS3404 [NZS 3404, 2007], Canada's CSA S16-09 [CSA S16-09, 2009] and the US AISC 341-10 [AISC 341-10, 2010] utilise the design philosophy often termed force-based design (FBD), which designs a structure for a set of reduced seismic forces depending on the structural system's ductility capacity by using either the equivalent lateral force or modal response spectrum methods of analysis. However, as discussed in Priestley [1993] and Priestley *et al.* [2007], this design approach possesses a number of fundamental

shortcomings, such as the use of unique force-reduction factors for structural systems regardless of the structural configuration or actual ductility capacity. Some codes have been modified to incorporate displacement-based design considerations for EBF link deformations, although it will be shown shortly that in the case of EBF design provisions in Eurocode 8 (EC8), there appears to be a need for improved consideration of displacements and deformations within the design process. Other energy-based methods have been proposed by Goel *et al.* [2009] and Sullivan [2011] which design the structure based on relating the input energy of the seismic action to the dissipated energy of the actual structure's plastic mechanism.

Some issues with current code design approaches particular to EBF systems are identified in the next section to provide motivation for the development of DDBD for such systems, where, by examining a series of case study SDOF EBFS designed using both European and US design code approaches, it is shown that comprehensive guidance ought to be given in the determination of link demands for EC8, while both US and European provisions show large variability in actual link demand to capacity ratios at the expected drift level. In light of this, a clarification has been proposed for EC8 to improve the estimation of link demands through the use of elastic analysis, as is normally carried in current code design. While it is shown how current methods can be modified and improved, it is also shown how the same issues of variability in actual design capacity do not exist with DDBD and resulting designs are more consistent in establishing link deformation demands, which is the main focus of this article. However, the DDBD procedure for EBFs recently proposed by Sullivan [2013] has not been extensively verified through detailed experimental calibration and numerical validation. This article therefore aims to refine the existing DDBD approach for EBFs by first proposing a newly calibrated numerical to accurately represent the hysteretic behaviour of the EBF system. Through this model, spectral displacement reduction factors are developed in support of DDBD and a series of case study structures are designed and analysed using nonlinear time history analysis to verify the performance of the proposed DDBD method. The work examines EBF structures with short links only, even though many of the observations would be relevant to EBFs with long links as well.

2.2 REVIEW OF CURRENT DESIGN CODE APPROACHES

This section reviews the current design approach to the seismic design of EBF structures and provides guidance on the use of elastic analysis to predict inelastic demands in the link element. This is done through examination of a series of single storey EBF structures that are designed using both European and US code provisions. The expected inelastic deformation capacity is determined via pushover analyses and compared to available capacity as predicted in order to highlight variability obtained using code approaches.

This analysis and discussion also provides the motivation for an alternative DDBD approach for the seismic design of EBFs.

2.2.1 Case Study Design of SDOF EBFs to EC8 and AISC 341-10

Table 2.1 shows a total of 16 different case study EBF structures designed to both European [EN 1998-1:2004, 2004] and US seismic design code provisions [AISC 341-10, 2010; ASCE 7-10, 2010]. The case study structures consist of a single storey EBF with varying link length (e), bay width (B), storey height (h), steel grade (f_y) and seismic mass (m). Each structure is designed to the soil type C design spectrum discussed further in Section 2.4.1.2, which has an equivalent peak ground acceleration on rock of 0.4g. It should be noted that this design spectrum is as per European seismic design provisions and is used for the calculation of seismic design forces for both EC8 and AISC design cases in order to maintain consistency. For each case, a short EBF link structure is assumed and an importance factor of 1.0 is used for both design codes. A behaviour factor (q) and displacement amplification factor (q_d) of 6.0 are used for European designs, as per EN 1998-1:2004 [2004], and a force reduction (R) and displacement behaviour factor (C_d) pair of 8 and 4 are used for US designs, as per [AISC 341-10, 2010], respectively. For both design code approaches, the design base shear is determined and the link members designed in accordance with EC8 and AISC for European and US designs, respectively. The surrounding elements such as the columns and brace members are designed in accordance with the relevant capacity design and member capacity checks for Eurocode 3 [EN 1993-1-1:2005, 2005] and AISC 360-10 [AISC 360-10, 2010] standards. For each of the structures designed, the lateral displacement was determined through an elastic analysis of the trialled section sizes and subsequently amplified by the relevant displacement amplification/behaviour factor for each design code. In the event of the link deformation check indicating a deformation capacity exceedance at the amplified elastic storey drift, the trial link section size was modified to increase strength and stiffness in the EBF. This iteration was necessary for a total of four cases for AISC designs, where a satisfactory design was established after typically two or three extra trials. In addition, the initial period was determined via eigenvalue analysis of the trial design and used in the subsequent iterations of design in place of the initial period estimate expressions provided by the design codes.

Table 2.1: Case study designs according to Eurocode 8 and AISC 341-10.

Case	e	B	h	f_y	m	Eurocode 8			AISC 341-10		
						Link/Beam	Brace	Column	Link/Beam	Brace	Column
	[m]	[m]	[m]	[MPa]	[t]						
1	0.4	7	3.2	275	150	HE140B	HE140B	HE100B	HE120B	HE140B	HE100B
2	0.6	7	3.2	275	150	HE140B	HE140B	HE100B	HE140B	HE140B	HE100B
3	0.8	7	3.2	275	300	HE200B	HE160B	HE120B	HE180B	HE160B	HE120B
4	1.2	7	3.2	275	300	HE280AA	HE180B	HE120B	HE260AA	HE160B	HE120B
5	0.4	7	3.2	460	250	HE140B	HE160B	HE120B	HE160B	HE180B	HE120B
6	0.6	7	3.2	460	250	HE160A	HE160B	HE120B	HE160B	HE160B	HE120B
7	0.8	7	3.2	460	500	HE200B	HE180B	HE140B	HE200B	HE200B	HE160B
8	1.2	7	3.2	460	500	HE260AA	HE200B	HE140B	HE260AA	HE200B	HE140B
9	0.4	5	3.2	460	250	HE160B	HE140B	HE120B	HE180A	HE140B	HE120B
10	0.6	5	3.2	460	250	HE160B	HE140B	HE120B	HE180A	HE140B	HE120B
11	0.8	5	3.2	460	500	HE240B	HE160B	HE160B	HE220B	HE160B	HE140B
12	1.2	5	3.2	460	500	HE240B	HE160B	HE160B	HE220B	HE160B	HE140B
13	0.4	5	4	275	150	HE180B	HE120B	HE140B	HE160B	HE120B	HE120B
14	0.6	5	4	275	150	HE180B	HE120B	HE140B	HE160B	HE140B	HE120B
15	0.6	5	4	275	300	HE280B	HE160B	HE160B	HE240B	HE140B	HE140B
16	1.2	5	4	275	300	HE280B	HE160B	HE160B	HE240B	HE140B	HE140B

The chord rotation demand determination is somewhat a source of discrepancy between design codes, as EC8 states (cl. 4.3.4) that "the displacements induced by the seismic

design action shall be calculated on the basis of the elastic deformations of the structural system" and that the link rotation can be found (cl. 6.8.2(10) and 6.6.4(3)) as the total link relative deflection at midspan divided by half the link length, while the commentary provided in AISC 341-10 states that the link demand should be computed as a function of the plastic interstorey drift. The amplification of elastic deformation demands for EC8 and the use of plastic storey drift for AISC 341-10 are utilised here in the estimation of link demands respectively in order to highlight an important difference. The demand to capacity ratio of the link plastic chord rotation is then determined for each approach, where the design plastic chord rotation capacity is taken as 0.08 rad for short links, as per both design codes. These ratios are plotted for each case in Figure 2.4 as the amplified elastic demand case, where it can be seen that all of the ratios are below unity, indicating that none of the designs are expected to exceed the link capacity, while the AISC approach of using plastic drift shows a marked difference in demand to capacity ratio estimation when compared to the amplified elastic link demand approach used in EC8.

2.2.2 Pushover Analysis of Case Study Structures

In order to perform a pushover analysis on the case study structures, a numerical model that can accurately represent the nonlinear behaviour of short link EBFs needs to be established. This section first presents such a model followed by the actual pushover analysis of the case study structures in order to evaluate their deformation capacity. This modelling will also be used for the nonlinear time history analyses carried out later in the paper.

2.2.2.1 *Link Model Overview*

In this work, a force-based fibre element model is developed in OpenSees [McKenna *et al.*, 2000]. To this extent, it is proposed that the behaviour of short links employed in EBFs can be represented numerically by using a force-based fibre-element to model axial and flexural behaviour, along with an uncoupled shear hysteretic behaviour to account for the flexibility and nonlinearity due to shear response in the link, as recommended by Malakoutian *et al.* [2013], but with the exception that the hysteresis rule used for the shear behaviour is changed to account for isotropic hardening and the plateau of the maximum shear force in the element. While the approach of Malakoutian *et al.* [2013]was shown to work well for a number of specimens, it does not seem appropriate to ignore the link's isotropic hardening behaviour, as is evident when consulting some of the observations made in the experimental tests discussed in the literature [Engelhardt and Popov, 1989b; Hjelmstad and Popov, 1983; Kasai and Popov, 1986; Mansour, 2010; Okazaki *et al.*, 2009; Popov *et al.*, 1987], where the hysteretic cycles were seen to "grow" with increasing deformation amplitude. The approach proposed here is to therefore use a different hysteresis rule and calibrate its parameters to give a behaviour that is more representative of that observed in previous experimental tests. The hysteretic rule adopted for the EBF

shear hinge is the Giuffre Menegotto-Pinto hysteresis rule, and a complete description of the relevant terms can be found in the OpenSees command manual [McKenna *et al.*, 2000]. The yield force input to the material model is the link yield force (V_y), with an initial stiffness of GA_v, where G is the steel shear modulus and A_v the shear area of the link, along with a post yield hardening ratio of 0.001. The elastic-plastic transition parameters (R0, cR1 and cR2) are taken as 20, 0.925 and 0.01, respectively, and the isotropic hardening parameters (a1, a2, a3 and a4) are taken as 0.02, 1, 0.02 and 1, respectively. This material is then aggregated into a fibre-element using the section aggregator tool within OpenSees.

2.2.2.2   *Validation with Experimental Results*

Using the link modelling parameters outlined in Section 2.2.2.1, results obtained using the proposed modelling approach are compared with existing experimental data to validate its performance as a modelling approach for short link EBFs. Experimental test results from Mansour [2010] and Okazaki *et al.* [2009] have been digitised and compared with the proposed model. Details of these test specimens are given in Table 2.2, where all tests adopted the EBF link loading protocol specified in the 2005 version of AISC 341 [AISC 341-05, 2005].

A comparison of the hysteretic responses of the links observed for each of the specimens listed in Table 2.2 and the proposed model is shown in Figure 2.2, and it can be seen that the proposed model and experimental results match very well. This is highlighted in the isotropic hardening of the links between cycles and the good representation of the stiffness transitions between the elastic and inelastic branches of behaviour. As such, it is concluded that the modelling parameters proposed here match actual experimental behaviour very well and are recommended for the fibre-element modelling of short link EBF structures. Note that the model is proposed for modelling of links with stable hysteresis and intermediate web stiffener detailing as per Eurocode, AISC and CSA requirements.

Table 2.2: Test specimen details for links used in model validation.

Reference	Specimen ID	Section Size	Link Length (mm)	Loading Protocol
Mansour [2010]	UT3A	W360x101	900	AISC 341-05
Mansour [2010]	UT3B	W360x101	900	AISC 341-05
Okazaki *et al.* [2009]	AISC-2	W18x40	980	AISC 341-05
Okazaki *et al.* [2009]	AISC-6	W10x68	980	AISC 341-05
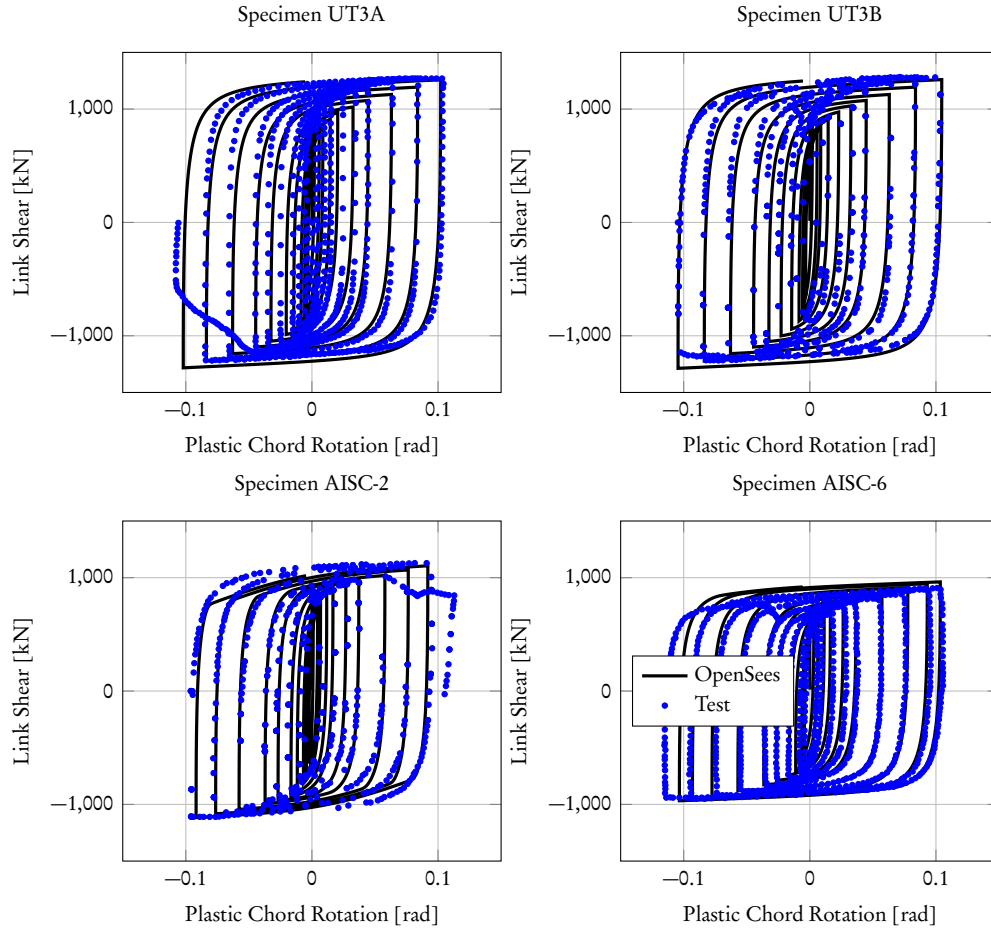
Figure 2.2: Validation of numerical model with experimental data.

2.2.2.3   *Single Storey Model*

The short link fibre-element modelling approach is now expanded into a single storey
EBF model to consider the behaviour of an entire storey of an EBF structure, not just
the principle component of its nonlinear behaviour. Figure 2.3 shows the proposed
model that includes the validated shear link model in addition to an arrangement of
beams and columns to represent a single storey of an EBF structure. Beam elements are
assumed to have pinned connections to the outer columns, as are the brace members. It
is acknowledged that connections between braces and the underside of the beam
members may consist of welded connections with a stiffened beam web to transfer large
shear forces from the braces through to the link, which has been demonstrated to be very
important for the performance of EBF systems through the observations of Kanvinde et

al. [2014] after the performance of an EBF during the 2011 Canterbury earthquake. However, the moments transferred through to the braces are generally quite low in comparison to the moments transferred to the outer beams and the governing forces acting through the braces are axial forces Nascimbene et al. [2012]. It is therefore deemed reasonable to idealise the brace to beam connection as a pinned connection and assume the moments developed in the links are transferred to the outer beams only, and this has therefore been the adopted approach for the model shown in Figure 2.3.
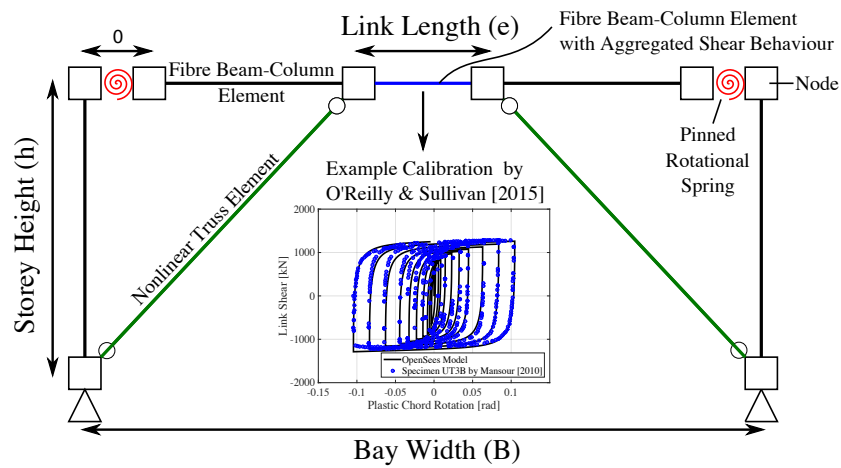
Figure 2.3: Single storey model for EBFs.

2.2.2.4 *Pushover Results*

Using the numerical model proposed in Section 2.2.2.3, an inelastic pushover analysis is performed on each of the designs listed in Table 2.1 to the expected interstorey drift demand, as determined from the code procedure. The resulting demand to capacity ratio of the actual link plastic chord rotations at this expected drift are then computed and plotted in Figure 2.4. As is immediately obvious from Figure 2.4, many of the EC8 design solutions exceed the link plastic chord rotation capacity at the expected drift and the amplified elastic link demand estimates are consistently underestimating the actual link demands, whereas the AISC designs are closer to a demand to capacity ratio of unity. Note that in order to arrive at the final AISC solutions, iteration was required in cases where the initial design solution (obtained using a force reduction factor of 8) was found to lead to excessive plastic chord rotation demands. This illustrates how the displacement-based considerations adopted in AISC 341-10 can effectively limit the plastic chord rotation demands to within an acceptable level. Also shown in Figure 2.4(b) are the displacement ductility capacities, obtained by pushing each of the EBF case study models to a plastic chord rotation of 0.08rad and dividing the observed storey displacement by the yield displacement of the EBF. As such, Figure 2.4(b) clearly

illustrates that the use of a single behaviour (or force reduction) factor does not result in consistent levels of ductility capacity for all EBF systems, while AISC does a reasonable job compared to EC8, which tends to expect much more ductility at the design displacement than is actually available. This variability in design demand to actual capacity highlights one of the principle shortcomings of current code-based seismic design discussed in Priestley *et al.* [2007], where the use of unique force reduction/displacement amplification factors is argued to be an illogical approach that does not consider geometrical or material property variations of the structure.
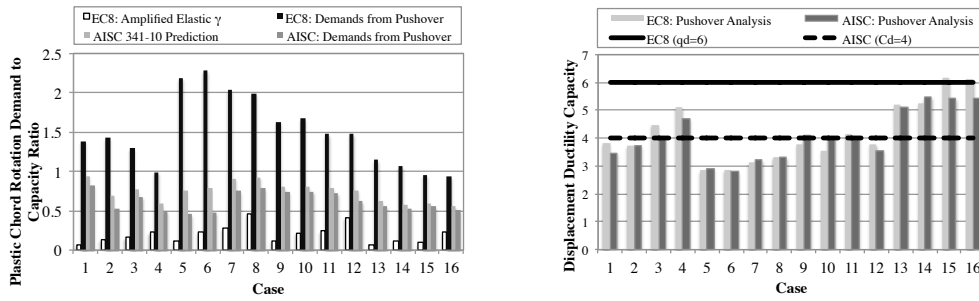
(a) Demand to capacity ratios. (b) Displacement ductility ratios.

Figure 2.4: Evaluation of European and US design solutions.

2.2.3 Improved Estimation of Link Plastic Deformation Demands in FBD

To better understand the results presented in the previous section and identify a means of improving the EC8 approach, note that the yield drift of a given storey of an EBF structure has three main components Sullivan [2013]: (i) flexibility of the link and beams (ii) flexibility of the brace elements and (iii) drift due to axial compression of the columns beneath the storey of interest. The drift contribution from each of these three components is determined here for three separate EBF structures to illustrate how each contributes to the interstorey drift of a storey within an EBF structure. The three example structures are taken from Sullivan [2013], with the modelling procedure described in Section 2.2.2.1 used to model the structures. A pushover analysis up to a displacement corresponding to 1% interstorey drift of each structure is performed and the individual components of storey drift are illustrated in Figure 2.5.

As previously mentioned, EC8 allows the computation of deformation demands in the inelastic range of response from elastic analysis assuming that the ratio between the contributions of the link, brace and column deformation are preserved at all displacements through the amplification of elastic demands. It is clear from Figure 2.5 that this is not the case, with the contribution of the brace and column deformations effectively plateauing after storey yield with the increasing drift contribution coming from

the deformation of the link. This means that the actual inelastic link demand is higher that what is determined by amplification of elastic deformation demand, which explains the observations in Figure 2.5, where the actual link demands observed from pushover analyses were of much higher magnitude than those estimated from elastic deformation amplification. This has been noted elsewhere [Kuşyilmaz and Topkaya, 2015] as somewhat of a grey area in code specifications with only the Commentary of AISC 341-10 providing some prescriptive guidance and EC8 not providing any explicit statement as to how to determine these demands.

(a) 1st Floor

(b) 2nd Floor

(c) 3rd Floor
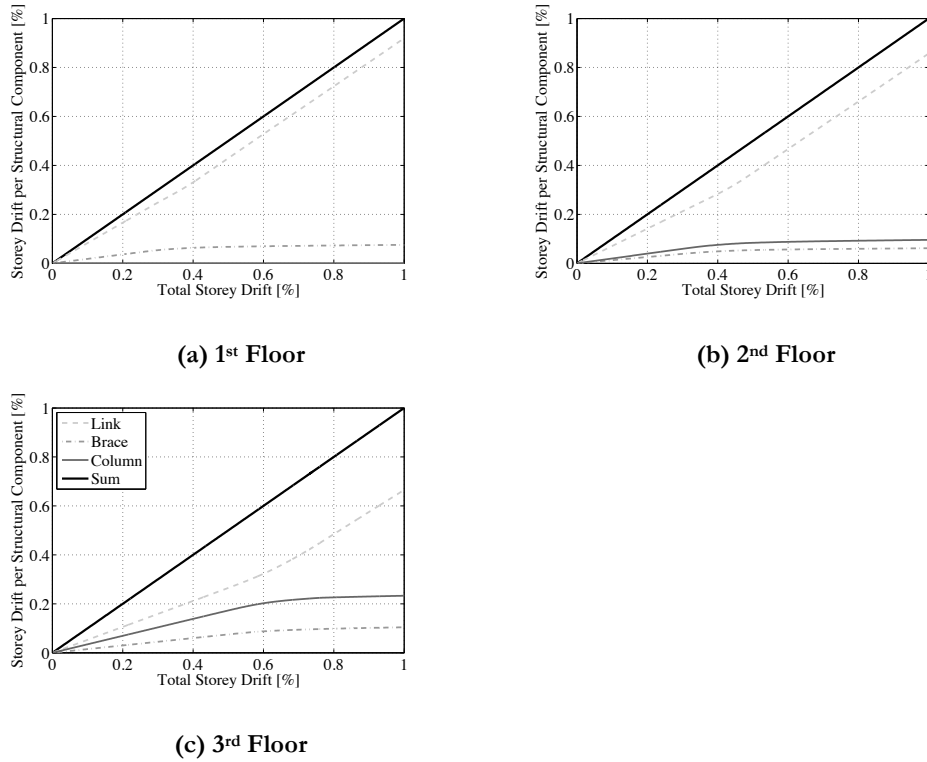
Figure 2.5: Interstorey drift contribution.

A simple expression can be derived to aid the calculation of actual link demand when using EC8. This relation, which is also described at least in principle in the Commentary of AISC 341-10, assumes that the contribution of the braces and columns to the interstorey drift remains constant upon yielding of the link element and the actual link plastic chord rotation demand for a storey i is given as:

$$\gamma_{p,i} = \frac{d_e B_i}{e_i h_i}(\mu_i - 1) = \frac{B_i(\theta_{\max,i} - \theta_{y,i})}{e_i}$$

<div align="right">Equation 2.1</div>

where d_e is the elastic relative storey displacement of a storey i determined from elastic analysis, μ_i is the storey ductility defined as the peak storey drift $\theta_{\max,i}$ divided by the storey yield drift $\theta_{y,i}$. Alternatively, the displacement amplification factors provided by design codes (C_d or q_d) may be used in the absence of a ductility term μ, even though this approach may be inaccurate for cases where one has links of different length in different bays of the same storey or different values of overstrength over the height of the structure. Note that the expression on the right in Equation 2.1 would be useful when non-uniform ductility demands are expected over the height of the structure. The discrepancy between amplified elastic link demands and actual link demands increases linearly with ductility, which is of great concern to the bottom storeys of MDOF EBF structures, which tend to be the critical storey with high ductility demand compared to the upper storeys. Thus, if the link chord rotation demand at the design level is currently being underestimated through the lack of explicit guidance in EC8, the probability of mechanisms such as soft-storey collapse increases as a result of the increased risk of link fracture due to excessive link chord rotation demands. Figure 2.6 demonstrates that by using Equation 2.1, the estimate of demand to capacity ratios greatly improves for the case of EC8, whereas AISC provisions already outline such a method in the commentary. The slight overestimation by Equation 2.1 in Figure 2.6 is attributed to the simplifying assumption of a purely plastic mechanism forming in the link without strain hardening. The results of Figure 2.6 illustrate that if the EC8 design procedure were to adopt Equation 2.1 to check plastic chord rotation demands, it would prompt changes to the vast majority of the initial design solutions presented earlier in Table 2.1 as these would be found to fail the link deformation demand limits. This highlights the urgent need to make changes to the current EC8 prescriptions. Note that once this issue is addressed, the best means of changing the structure to reduce excessive chord rotation demands may still not be clear and the designer must go through a series of revisions to satisfy both force and displacement requirements; it was found that the AISC cases in Section 2.2.1 typically took 2 or 3 iterations to complete. Such an exercise can be quite time consuming and in addition to design calculations, the designer must also have prepared an analytical model of the structure to determine the elastic displacements and deformation of the structure. This is one of the main benefits of moving towards the displacement-based design approach presented in the following section, where the focus is to control link deformations rather than forces and a design solution can be obtained in a single step rather that a series of iterations requiring analytical software.

(a) Eurocode 8   (b) AISC 341-10
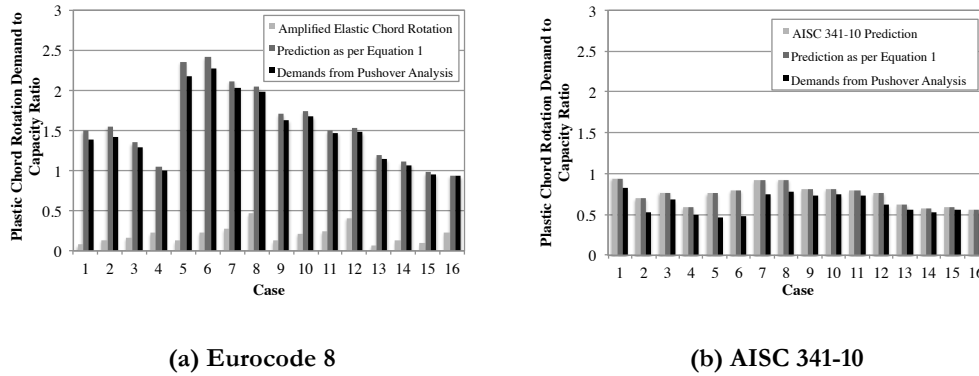
Figure 2.6: Demand to capacity ratio of link plastic chord rotations.

2.3 DIRECT DISPLACEMENT-BASED DESIGN OF ECCENTRICALLY BRACED FRAMES

The previous section has demonstrated that there is some discrepancy with current EC8 design guidelines for EBF systems with different procedures for determining expected design deformations and considerable effort required to give a satisfactory design. Such issues motivate the development of alternative seismic design approach and in this section, the DDBD procedure of Priestley *et al.* [2007] and extended by Sullivan [2013] to EBFs is reviewed and refined.

2.3.1 Overview of DDBD

The DDBD methodology Priestley *et al.* [2007] allows for the design of a structure to specified target displacements and thus, a specific performance level that can be related to chord rotation and interstorey drift limits. The key steps of DDBD are summarised in Figure 2.7, where an SDOF system is used to represent an MDOF system at maximum displacement in its first fundamental mode of response (Figure 2.7 (a)), which for the specific case of EBFs will be discussed in Section 2.3.5.1. Figure 2.7(b) shows the SDOF representation of the structure as an equivalent linear system with secant stiffness to the design displacement. To account for the effects of energy dissipation and nonlinear response, the equivalent linear SDOF is attributed an equivalent viscous damping coefficient (as per Priestley *et al.* [2007]) or a displacement reduction factor (used here) as a function of the level of ductility demand, as shown in Figure 2.7(c) and discussed further in Section 2.3.3. For the case of EBF structures, a DRF specific to EBFs is developed in Section 2.3.3 as a part of this paper. The target displacement ductility is a function of the system yield displacement and target displacement. The yield displacement can be typically found from geometry and material strain definitions, whereas the target displacement for EBFs is determined from plastic chord rotation or interstorey drift limits, which means that the structure's displacements are a key definition

of the design process that can be adjusted to control certain limits states. As shown in Figure 2.7(d), the design displacement is then used in conjunction with the DRF to enter the DRF-reduced spectral displacement response spectrum in order to determine the required effective period T_e of the equivalent linear system. Using the effective period, the effective stiffness, K_e, of the SDOF system at the target displacement is determined from the expression given in Figure 2.7(b), where m_e is the effective mass. The product of effective stiffness and the design displacement, Δ_d, provides the design base shear V_b as per Figure 2.7(b). This is therefore a direct method that does not require iterations of initial period or elastic analysis to determine design displacement demand and a complete design can be obtained on one single spreadsheet.

To extend the DDBD approach to MDOF structures, the substitute structure concept of Gulkan and Sozen [1974] and Shibata and Sozen [1976] is used to identify the SDOF properties of a MDOF system assuming a certain displaced shape at maximum response. This is used to find the design target displacement, Δ_d, of the structure and its effective mass, m_e that are used in the DDBD process outlined previously. The expressions for these terms are given in Figure 2.7(a) where n is the number storeys in the structure, Δ_i comes from the design displacement profile for the structure (see Section 2.3.5.1) and H_i is the storey elevation, as outlined in Priestley *et al.* [2007].

$$\Delta_d = \frac{\Sigma m_i \Delta_i^2}{\Sigma m_i \Delta_i}$$

$$m_e = \frac{\Sigma m_i \Delta_i}{\Delta_d}$$

$$V_b = K_e \Delta_d$$

$$K_e = 4\pi^2 \frac{m_e}{T_e^2}$$

(a) MDOF to SDOF Substitute Structure

(b) Equivalent Linearisation of SDOF System

$$\mu = \Delta_d / \Delta_y$$

(c) Displacement Reduction Factor

(d) Design Displacement Spectrum
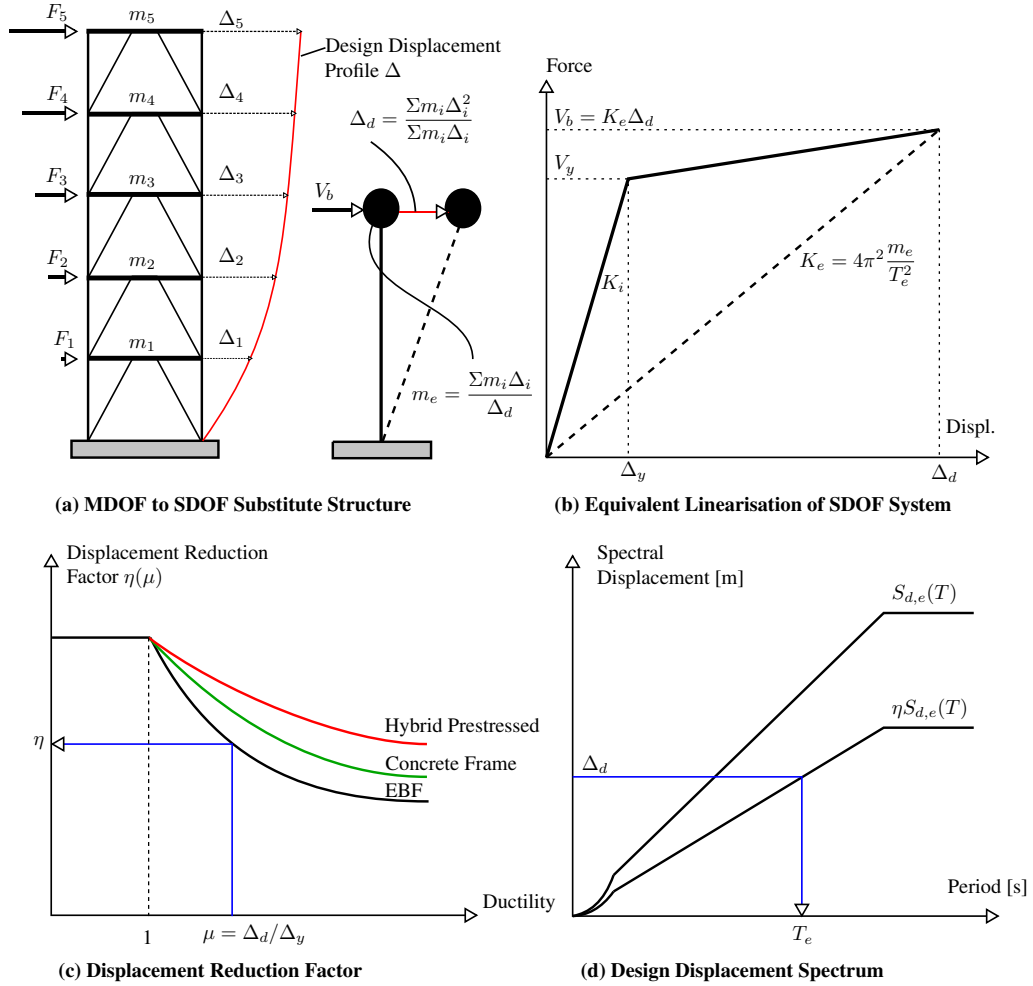
Figure 2.7: Fundamental aspects of the DDBD procedure [Priestley *et al.*, 2007].

2.3.2 DDBD of SDOF EBF Structures

2.3.2.1 *EBF Storey Displacement Capacity*

The first step in DDBD of SDOF EBFs is the determination of the design displacement and ductility as a function of the storey drift through the expressions:

$$\Delta_d = \theta_d h$$

Equation 2.2

$$\mu = \theta_d \Big/ \theta_y \qquad\qquad \textbf{Equation 2.3}$$

where Δ_d is the design displacement, h is the interstorey height at storey i and the design drift θ_d is determined as the drift capacity $\theta_{c,i}$. The drift capacity of a given storey in an EBF is computed as the sum of the yield $\theta_{y,i}$ and plastic $\theta_{p,i}$ storey drift components. As mentioned previously, the storey yield drift of an EBF structure is principally composed of deformations of three components: (i) link (and beam) bending and shear deformation $\theta_{link,i}$, (ii) brace axial deformation $\theta_{br,i}$ and (iii) column axial deformation $\theta_{col,i}$. These individual contributions to the yield drift of an EBF are discussed in detail in Sullivan [2013] and the final expressions describing each contribution are noted here for brevity and completeness as:

$$\theta_{y,i} = \theta_{link,i} + \theta_{br,i} + \theta_{col,i} \qquad\qquad \textbf{Equation 2.4}$$

$$\theta_{y,i} = \frac{f_y A_{v,i} e_i}{\sqrt{3}(B - e_i)}\left(\frac{e_i(B - e_i)}{12EI_{zz,i}} + \frac{1}{GA_{v,i}}\right) + \frac{2k_{br,i}\varepsilon_y}{\sin(2\alpha_i)} + \frac{2k_{col,i-1}\varepsilon_y H_{i-1}}{B} \qquad \textbf{Equation 2.5}$$

where the general notation is as illustrated in Figure 2.1, with $I_{zz,i}$ representing the second moment of area of the beam about the major axis, E and G are the elastic and shear moduli of steel, respectively, $A_{v,i}$ is the shear area of the link element, f_y is the steel yield strength, ε_y is the steel yield strain, α is the brace angle and $k_{br,i}$ represents the ratio of the actual strain in the brace to the yield strain, which can be computed as the axial force ratio in the brace, as follows:

$$k_{br,i} = \frac{N_{Ed,br,i}}{N_{c,Rd,br,i}} \qquad\qquad \textbf{Equation 2.6}$$

where the terms $N_{Ed,br}$ represents the DDBD first mode axial force on the brace member and not the final capacity design axial force since the expected brace strain for DDBD is required here. The term $N_{c,Rd,br}$ represents the compressive axial capacity (Af_y) of the brace section, not to be confused with the member buckling capacity.

The right most term in Equation 2.5 includes a storey drift term component due to column axial deformations. For SDOF EBF systems, this term can be taken as zero. For MDOF systems, it should be computed noting that the term H_{i-1} is the elevation of the floor below the one being considered and $k_{col,i-1}$ represents the average expected column axial force to the yield of these column sections, similar to the k_{br} ratio shown above. As

there can be many storeys below the storey i being considered, there are many ratios of expected to capacity axial load ratios, which were found to typically vary from 0.3 to 0.4. The average ratio can therefore used in Equation 2.5, which is calculated by:

$$k_{col,i-1} = \frac{1}{i-1} \sum_{j=1}^{i-1} \frac{N_{Ed,col,i}}{N_{c,Rd,col,i}}$$

<div align="right">**Equation 2.7**</div>

Note that the k_{br} and k_{col} ratios in Equation 2.6 and Equation 2.7 are iterative and may appear somewhat difficult to establish but are actually completely within the designer's control. This is because the designer chooses the final column and brace sections and therefore, if desired, could select final column and brace sections that respect the k_{br} and k_{col} values adopted during DDBD, provided that the final member sizes are also checked for capacity design actions. Since some iteration may result during the determination of both k_{br} and k_{col} acceptable tolerances are suggested to be of the order of 0.01 which is typically achieved quite quickly after just a few iterations. This was demonstrated through example application in the Appendix of Sullivan [2013], where just two iterations were required. However, should a design spreadsheet be prepared, the initial values for k_{br} and k_{col} can be directly linked to the computed values from the selected braces and column section sizes, meaning that the spreadsheet automatically updates itself for instantaneous convergence.

As the total drift capacity of an EBF is a combination of the yield drift plus the plastic drift capacity, it is given by:

$$\theta_{c,i} = \theta_{y,i} + \theta_{p,i}$$

<div align="right">**Equation 2.8**</div>

$$\theta_{c,i} = \frac{f_y A_{v,i} e_i}{\sqrt{3}(B-e_i)} \left(\frac{e_i(B-e_i)}{12EI_{zz,i}} + \frac{1}{GA_{v,i}} \right) + \frac{2k_{br,i}\varepsilon_y}{\sin(2\alpha_i)} + \frac{2k_{col,i-1}\varepsilon_y H_{i-1}}{B} + \frac{e_i\gamma_p}{B}$$

<div align="right">**Equation 2.9**</div>

where γ_p is the link plastic chord rotation capacity, for which current code defined limits for design are given as 0.08 rad and an ultimate limit of 0.10 rad is specified for both EC8 and AISC 341-10.

2.3.2.2 *Equivalent Viscous Damping and Spectral Displacement Reduction Factors*

In addition to the design displacement and ductility, one requires knowledge of the equivalent viscous damping or displacement reduction factor (DRF) for the DDBD of

EBFs, which is illustrated in Figure 2.7(c) to be directly related to ductility (μ). Section 2.3.3 discusses the development of a DRF expression for EBF systems, which is given here as:

$$\eta = \begin{cases} 1.0 & for \quad \mu \leq 1 \\ 2.16\exp(-1.61\mu) + 0.56\exp(0.01\mu) & for \quad \mu > 1 \end{cases}$$

Equation 2.10

2.3.2.3   *Effective Period and Base Shear*

The next step of the EBF design is to compute the effective period and design base shear. This can be done using the ductility dependent DRF determined from Equation 2.10 to reduce the design spectrum, as outlined in Figure 2.7(d). Using this reduced design spectrum, the required effective period (T_e) is obtained by entering the spectrum with the target design displacement (Δ_d) and finding the corresponding period on the reduced spectrum, as illustrated in Figure 2.7(d). As per Figure 2.7(b), the required effective stiffness for the equivalent linear SDOF system is given by:

$$K_e = \frac{4\pi^2 m_e}{T_e^2}$$

Equation 2.11

and the base shear is then determined, with the inclusion of additional capacity to account for P-Delta effects, as follows:

$$V_b = K_e \Delta_d + C \frac{\sum_{i=1}^{n} P_i \Delta_i}{H_e}$$

Equation 2.12

$$C = \begin{cases} 1 & for \quad \dfrac{m_e g}{K_e H_e} \geq 0.05 \\ 0 & for \quad \dfrac{m_e g}{K_e H_e} < 0.05 \end{cases}$$

Equation 2.13

where P_i represents the seismic weight at a given floor i and C is a P-Delta effect coefficient, whose limits are proposed by Priestley *et al.* [2007] and Sullivan *et al.* [2012] for steel structures as shown.

2.3.2.4 *Link Member Sizing*

Using the design base shear, the design shear forces ($V_{Ed,link,i}$) on the link elements can be determined from equilibrium, which for a given storey (also in MDOF systems) is then:

$$V_{Ed,link,i} = \frac{V_i h_i}{B}$$

Equation 2.14

In order to size sections for these links, the actual strength of the link should be determined at the design plastic chord rotation. This requires knowledge of the strain-hardening provided by the section at the design level of deformation. Using the hysteretic model proposed for EBFs in Section 2.2.2.1, this expected overstrength is in the region of 1.25 and as such is proposed. It is acknowledged that this value of 1.25 is somewhat smaller than the values discussed in the literature [Della Corte *et al.*, 2013; Mohebkhah and Chegeni, 2014], but it is envisaged that these values represent the best comparison to the value obtained from the numerical model that is used to evaluate the structure. The actual strength increase with deformation may, however, also be affected by slab resistance (not modelled) and therefore the value indicated in Equation 2.15 may need to be revised in the future should significant slab interaction be anticipated. Considering the above, the resistance offered by the link ($V_{Rd,link,i}$) at the design drift level is given as:

$$V_{Rd,link,i} = \begin{cases} \dfrac{\theta_i}{\theta_{y,i}} V_{y,link,i} & for \quad \mu \le 1 \\ \left(1 + 0.25 \dfrac{\gamma_{p,i}}{\gamma_p}\right) V_{y,link,i} & for \quad \mu > 1 \end{cases}$$

Equation 2.15

where $\gamma_{p,i}$ is the plastic chord rotation demand for level i and γ_p is the design plastic chord rotation capacity, typically taken as 0.08 rad as outlined previously.

In order to provide a uniform distribution of design strength in each storey of MDOF systems, the overstrength of the EBF system, defined as the ratio of the actual resistance provided to the design force, is limited to avoid providing excessive overstrength in certain storeys and hence a concentration of damage in the adjacent storeys. EC8 specifies that the additional overstrength of the link members (Ω) be no more than 1.25 times the required design strength to avoid such issues, which is adopted here.

2.3.2.5 *Capacity Design*

The final step in the seismic design process is to confirm the sizes of the brace and column sections and any other elements or connections not intended to yield during seismic response through the application of capacity design rules. In order to do this, the actual forces generated by the yielding link elements needs to be properly identified and amplified so that the sizing of the capacity design protected elements is sufficient to ensure they remain elastic during seismic response. Amplification factors for brace and columns vary between 1.375 and 1.5 times the expected force generated by the link members [AISC 341-10, 2010; CSA S16-09, 2009; EN 1998-1:2004, 2004; NZS 3404, 2007], where a value of 1.5 times the force developed in the link ($V_{Rd,link,i}$) was proposed in Sullivan [2013] for the DDBD of EBFs and this same value is adopted here for simplicity. Once amplified actions have been found, standard code expressions for member resistances can be applied to verify the section resistances.

2.3.3 Development of a Spectral Displacement Reduction Factor for EBFs

The concept of equivalent viscous damping (EVD) was first introduced by Jacobsen [1930], where the hysteretic damping associated with the energy dissipation in nonlinear systems was related to the area enclosed by the hysteretic loop. Jacobsen [1930] proposed that this EVD term could be equated to the energy absorbed by the system during a cycle of steady-state harmonic response. This assumption of steady-state response was subsequently shown by Dwairi *et al.* [2007] to be an unrealistic assumption for systems subjected to earthquake ground motions. Given this limitation with the classical EVD definition, Grant *et al.* [2005], Dwairi *et al.* [2007] and Pennucci *et al.* [2011] calibrated EVD expressions to a variety of hysteresis rules that match results obtained using nonlinear time history (NLTH) analyses. This EVD was a combination of both the elastic damping term, typically taken as 5%, and the hysteretic damping resulting from hysteretic energy dissipation. This EVD term was then used in conjunction with a damping-dependent displacement scaling factor (DSF) to relate the design displacements with and effective period for the substitute structure. The damping dependent DSF expression suggested by Priestley *et al.* [2007] for use in DDBD is that found in the previous 1998 version of the Eurocode, as this was found to provide the best inelastic displacement estimates when used together with the EVD expressions developed by Grant *et al.* [2005] and Dwairi *et al.* [2007].

More recent research by Pennucci *et al.* [2011] has shown that the use of separate DSF and EVD expressions results in a sensitivity as to the characteristics of the ground motions used to calibrate the EVD expression. Since the EVD expressions outlined in Priestley *et al.* [2007] are a function of ductility and the DSF is a function of EVD, Pennucci *et al.* [2011] proposed that the DSF be related directly to the ductility, instead of calibrating an intermediate EVD term. Pennucci *et al.* [2011] subsequently found that by

relating a displacement reduction factor (DRF) directly to the ductility, the expression was relatively insensitive to the type of ground motions used, as was not the case with EVD expressions. Pennucci *et al.* [2011] thus proposed a revised set of DRFs for a series of hysteretic types that relate the DRF directly to the ductility. Three DRF curves are shown in Figure 2.7(c) for hybrid prestressed and concrete frames, for which expressions were calibrated by Pennucci *et al.* [2011], and for EBF systems for which no expression has been explicitly proposed to date. However, since a hysteretic model for short EBF links has been proposed in Section 2.2.2.1, this section presents the calibration of a new expression for short link EBFs based on this experimentally calibrated numerical model.

2.3.3.1 *Proposed Methodology*

In order to calibrate a DRF for an EBF system characterised by the numerical modelling parameters outlined in Section 2.2.2.1, a number of NLTH analyses are carried out on a series of SDOF oscillators. This is done to compute the maximum displacement of a nonlinear SDOF system and relate this to the maximum displacement obtained using an equivalent linear SDOF system using an appropriate DRF. By assuming two initial sets of parameters, initial period (T_i) and force reduction factor (R), the properties to be supplied to the hysteretic model described in Section 2.2.2.1 can be determined, where the force reduction factor (R) represents the ratio between the inelastic yield force of the SDOF oscillator and the elastic force associated with the elastic spectra of the ground motion. This way, when the actual inelastic response of the SDOF oscillator is determined for a given ground motion, the corresponding ratio of elastic to inelastic displacement is determined. The variation of both initial periods and force reduction factors lead to a data set with a range of effective periods (T_e) and ductility demands (μ), defined at the absolute maximum response of the SDOF oscillator, which are of principle interest in DDBD. Since early work on the calibration of EVD expressions by Grant *et al.* [2005] showed that the EVD of a hysteresis rule can be sensitive to the effective period of the oscillator, this needs to be considered in this calibration. The period dependency of the EVD expressions calibrated by Grant *et al.* [2005] showed that for effective periods greater than 1 second, this dependency is relatively insignificant and could be ignored for practical design purposes since effective periods in DDBD tend to be longer than 1 second.

The calibration procedure adopted here is outlined in Figure 2.8, where each combination of initial period, force reduction factor and ground motion record leads to a single data point on the plot of DRF versus ductility. The initial parameters to be input into the hysteretic model are first computed and the dynamic analysis is run for the combination of initial period, force reduction factor and individual ground motion to give the actual displacement for the nonlinear SDOF system, Δ_a. From this, the effective period to the actual displacement is computed and the spectral displacement at the effective period is

taken from the spectrum to give the equivalent elastic SDOF's displacement. By comparing the ratio of the actual nonlinear SDOF's displacement with the equivalent elastic system's, the DRF is computed, as shown in Figure 2.8. In addition to computing the median DRF from each of the simulations described above, the distribution of DRF versus ductility can also be considered by performing vertical statistics on the dataset, as outlined in Figure 2.8. This is particularly useful when characterising the dispersion of the DRF to assist in making probabilistic considerations within displacement-based assessment methods such as Welch *et al.* [2014] and Sullivan *et al.* [2014]. The ground motion records used in this study consist of the artificial set proposed in a similar study by Pennucci *et al.* [2011] and the four sets of ten natural ground motion records outlined in Maley *et al.* [2013].
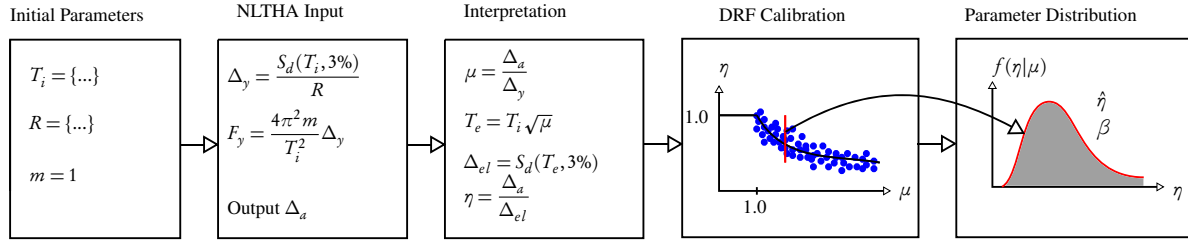
Figure 2.8: DRF calibration methodology.

Since the calibration looks at the variation in SDOF properties, an appropriate range of values must be determined for the calibration. These are as follows:

- A total of 50 effective periods (T$_i$) are considered between 0.2 and 4 seconds, as this corresponds to a reasonable range of expected values in EBF structures.
- A total of 50 force reduction factors (R) are considered between 1 and 5, as this is deemed to be an acceptable range for the EBF system.
- A total of 50 ground motions are selected, including a set of 10 artificial records and 40 natural ground motions records covering both EC8 soil types A and C, and displacement spectrum corner periods of 4 and 8 seconds [Maley *et al.*, 2013].

Note that DRF data was only maintained if the effective period lay prior to the corner period of the displacement spectrum, so as not to be influenced by spectral shape effects identified by Pennucci *et al.* [2011].

Using the above parameters, the SDOF model can be constructed for NLTH analyses with an appropriate ground motion record and the analysis is carried out at a numerical integration time step of 0.002s. The elastic damping (ξ) considered for the SDOF system was set to 3% and this was applied as tangent stiffness proportional damping following

the recommendations of Priestley *et al.* [2007]. Since a typical value for the elastic damping in steel structures is 3% as opposed to 5%, which is more typical of reinforced concrete structures [Chopra, 2012], a value of 3% has been adopted here. In order to construct the 3% damped elastic design spectrum from those specified in design codes, the displacement scaling factor proposed in Eurocode 8 may be used, which is given as follows:

$$R_\xi = \sqrt{\frac{10\%}{5\% + \xi}}$$

<div align="right">**Equation 2.16**</div>

where for a damping of 3%, Equation 2.16 increases the spectral demands accordingly. Hence, the DRF expression presented here is only applicable for the design of structures where 3% tangent stiffness proportional elastic damping is considered in conjunction with a typical 3% damped elastic spectrum.

2.3.3.2 *Calibration of DRF Expression for EBF Structures*

Collecting the data from the suite of NLTH analyses previously highlighted, the complete dataset is compiled and shown in Figure 2.9(a). In order to examine the dataset in detail, the data is binned at ductility increments of 0.1, which allows the computation of the median and dispersion values of DRF versus ductility. The median value of the data is determined from each of the bins and plotted in Figure 2.9(a), for which the DRF expression to be used in DDBD will be fitted. Also shown in Figure 2.9(a) is an example of the distribution of the DRF at a ductility of 2.15. A lognormal distribution is assumed for the data, which passes the Lilliefors goodness-of-fit test at the 5% significance level. Figure 2.9(b) shows the dispersion associated with each of the data bins versus ductility, where it is seen to plateau at around 0.35 above a ductility of 1.5, where the reduction in dispersion decreases as the ductility approaches unity, since no dispersion is expected for linear elastic systems. The dispersion is reported here as it is expected that it could be useful for the eventual realisation of probabilistic displacement-based design and assessment methods (see, for example, Welch *et al.* [2014]). The value of 0.35 is reasonably high but is also in line with values proposed in FEMA P-58 [FEMA P58-1, 2012], suggesting that the results obtained here are in line with those obtained elsewhere.

(a) DRF vs. ductility   (b) DRF dispersion vs. ductility
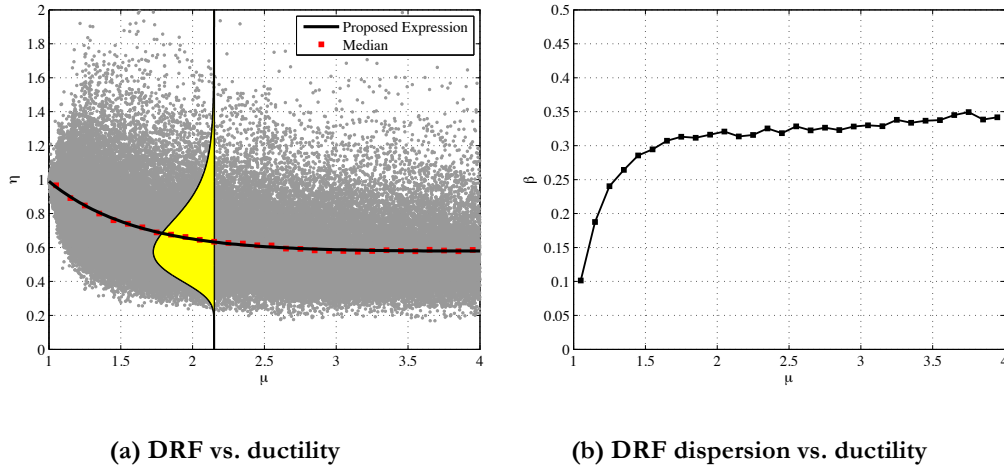
Figure 2.9: DRF results.

Using the median values form each of the bins plotted in Figure 2.9(a), an expression can be fitted in order to provide a simple expression to calculate the DRF for EBF structures. This expression, which is also plotted in Figure 2.9(a), is given previously in Equation 2.10 and corresponds to the DRF expression to be used for EBF structures, assuming 3% tangent stiffness proportional elastic damping and using the modelling recommendations of Section 2.2.2.1. As is evident from Figure 2.9(a), the proposed expression fits the median of the data very well.

2.3.4 Case Study Design and Assessment of SDOF EBFs using DDBD

Using the DDBD procedure for SDOF structures outlined in Section 2.3.2 in conjunction with the calibrated DRF expression of Section 2.3.3, the case study structures of Section 2.2.1 can be redesigned using DDBD. The geometry, material properties and design seismicity of the case studies is maintained and the resulting designs are shown in Table 2.3. As outlined in Section 2.3.2, these structures were sized by first determining their yield drift and drift capacity as per Equation 2.5 and Equation 2.9, respectively. The resulting ductility is used to calculate the corresponding DRF in accordance with Equation 2.10, and the design base shear is determined from Equation 2.12. The EBF link members are the sized according to Equation 2.14 and the resulting designs are shown in Table 2.3. In general, it is observed that the section sizes resulting from DDBD are on average a little larger than those resulting from using Eurocode 8 and ASCE 7-10.

<p align="center">**Table 2.3: Case study designs according to DDBD.**</p>

Case	e [m]	B [m]	h [m]	f_y [MPa]	m [t]	Link	Brace	Column
1	0.4	7	3.2	275	150	HE260B	HE200B	HE160B
2	0.6	7	3.2	275	150	HE260B	HE200B	HE160B
3	0.8	7	3.2	275	300	HE240M	HE200M	HE200B
4	1.2	7	3.2	275	300	HE240M	HE200M	HE200B
5	0.4	7	3.2	460	250	HE240B	HE240B	HE160B
6	0.6	7	3.2	460	250	HE240B	HE220B	HE160B
7	0.8	7	3.2	460	500	HE240M	HE220M	HE200B
8	1.2	7	3.2	460	500	HE240M	HE220M	HE200B
9	0.4	5	3.2	460	250	HE200M	HE200B	HE180B
10	0.6	5	3.2	460	250	HE200M	HE200B	HE180B
11	0.8	5	3.2	460	500	HE300M	HE240B	HE240B
12	1.2	5	3.2	460	500	HE260M	HE220B	HE220B
13	0.4	5	4	275	150	HE240M	HE200B	HE200B
14	0.6	5	4	275	150	HE240M	HE200B	HE200B
15	0.6	5	4	275	300	HE360M	HE220B	HE260B
16	1.2	5	4	275	300	HE280M	HE200B	HE220B

Similar to Section 2.2.2, a pushover analysis on each of the case study structures presented in Table 2.3 is performed using the numerical model outlined in Section 2.2.2.1 to evaluate the demand to capacity ratio of the link plastic chord rotation at the design drift level. By setting the design procedure up in terms of displacements, DDBD aims to define the target displacement of the structure in terms of material limit states and expected ductility capacities, which are then used to determine design forces and size the structure in one step, as opposed to the iterative procedures outlined in design codes if the deformation limits are not respected. For each of the designs, the SDOF EBF is subjected to a displacement controlled pushover analysis to the design drift. At this drift, the link plastic chord rotation is noted and compared with the plastic chord rotation capacity of 0.08rad specified for short link EBFs. Figure 2.10 shows the ratio between these two, where it is immediately obvious that DDBD provides design solutions that are all within the specified capacity, but also consistently at the same level of demand/capacity ratio, with the ratio always just less than unity. When comparing to the designs outlined in Section 2.2.1, it is seen how the DDBD method presented here provides a more consistent design solution than existing design code approaches, which had a large variation in demand to capacity ratio for different configurations and tended

to initially exceed the design link capacity, especially in the case of EC8. In addition, no analysis program was required to design the sections (apart from the pushover analyses to evaluate the design solutions and provide the data shown in Figure 2.10). In addition, no iteration of designs was required and a complete design can be carried out on one single design spreadsheet. This highlights the added benefits of using DDBD for the seismic design of EBF structures.
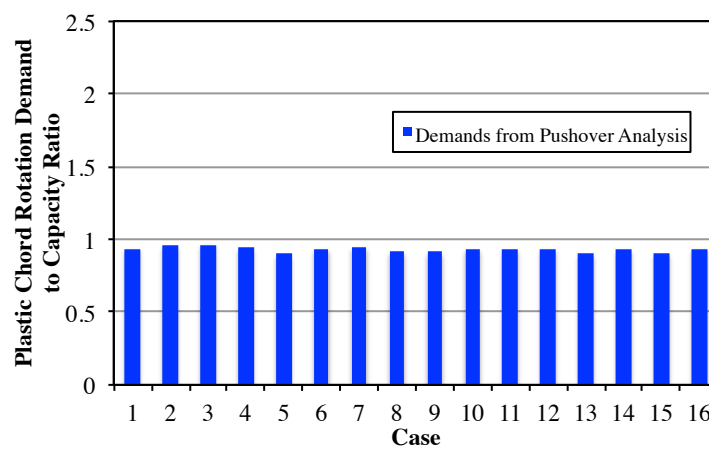
Figure 2.10: Demand to capacity ratio of link plastic chord rotation of DDBD solutions.

2.3.5 Extension of DDBD to MDOF Structures

The previous section outlined the process of designing a SDOF EBF structure for a specified target displacement and how case study designs showed that this approach led to more consistent design solutions than current design code approaches. This section takes this method for SDOF systems and extends it to the design of MDOF EBF structures. The following subsections describe the relevant additions to complete the DDBD process or MDOF EBFs with reference to Figure 2.7. However, for a detailed step-by-step description of the methodology, readers are referred to Sullivan [2013].

2.3.5.1 *Design Displaced Shape Profile*

In addition to the yield drift and drift capacity of an individual storey, a target displaced shape is required for MDOF EBF structures, with the displaced shape scaled to the limit-state drift capacity of the most critical floor in the building. Sullivan [2013] proposed the following expression for the limit-state profile, which gives a linear displaced shape at elastic displacement levels and a more parabolic shape for higher intensity levels:

$$\Delta_{ls,i} = \begin{cases} \min(\theta_c)H_i & \text{for} \quad \min(\theta_c) \leq \min(\theta_y) \\ \min(\theta_c)H_i + \big(\min(\theta_c) - \min(\theta_y)\big)H_i\dfrac{2H_n - H_i}{2H_n - H_1} & \text{for} \quad \min(\theta_c) > \min(\theta_y) \end{cases}$$
<div align="right">**Equation 2.17**</div>

where the terms $\min(\theta_y)$ and $\min(\theta_c)$ refer to the minimum value of both yield and capacity drift calculated over the entire height of the structure. This expression was shown by Sullivan [2013] to match the displacement profiles obtained at various intensities for a 6-storey EBF structure tested by Whittaker *et al.* [1987] and because the design displacement profile becomes more non-linear at increasing levels of ductility demand, it is considered more accurate than the invariant displacement profiles predicted from elastic modal analyses (currently used in code design methods).

2.3.5.2 *Higher Mode Effects*

In addition to the definition of the displaced shape of the EBF for an assumed first mode structural response, consideration must also be given to the possibility of higher modes of vibration increasing storey drift demands. In order to account for this higher mode response, two steps are taken in the DDBD procedure to ensure excessive drifts do not develop in the upper floors:

1. The target limit-state displaced shape is scaled down to account for increased drifts associated with higher mode response (see Figure 2.11), so that as the drift contribution of the higher modes increases, the first mode displaced shape is scaled down by such an amount that results in the combined drift of all modes remaining within the target drift limits.
2. A fraction (typically 10%) of the design base shear is lumped at the roof level when setting the required design strength distribution to increase strength in upper floors and achieve relatively uniform drift demands over the structure height.

This scaling referred to in point 1 above is done by the application of the scaling factor ω_θ, in line with recommendations of Sullivan *et al.* [2012], which is illustrated in Figure 2.11 for EBFs, to the limit state displaced shape $\Delta_{ls,i}$ to give the design displaced shape as:

$$\Delta_i = \omega_\theta \Delta_{ls,i}$$
<div align="right">**Equation 2.18**</div>

As shown in Figure 2.11, this higher mode scaling factor is a function of the number of storeys (n) in the structure. For the adjustment of the lateral force vector to ensure more uniform displacement response (point 2 above), this will be discussed in tandem with the discussion of the lateral force application in Section 2.3.5.4.
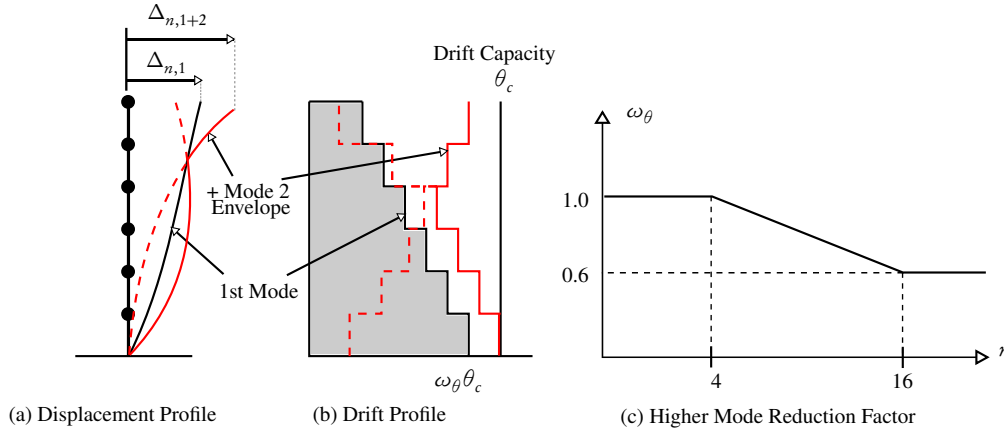
Figure 2.11: Accounting for higher mode influence on EBF interstorey drift profiles.

2.3.5.3   *DDBD of EBFs Using Proposed DRF*

Section 2.3.3 proposed a new DRF expression for EBF structures. In order to implement Equation 2.10 into DDBD, some additional considerations are required when designing MDOF EBF structures. Equation 2.10 relates the μ of the EBF to the η and for the case of a SDOF EBF, the ductility varies along the height of the structure. Sullivan [2013] proposed to find the equivalent SDOF system's ductility (μ) and implement this to find the equivalent SDOF system's DRF (η). However, since the design displaced shape of the EBF is proposed to be of a parabolic shape, the upper storeys of high-rise EBF's tend to remain elastic for the design displacement. This is observed in the design case study structures summarised in Table 2.5 and Table 2.6. If the equivalent SDOF system's μ is calculated through the weighting of work done at each level of MDOF structure and then used in Equation 2.10, for which an equivalent SDOF η greater than unity is computed, this inherently assumes that the expression given in Equation 2.10 for μ greater than 1 is valid over all ductility values, which according to Equation 2.10 is not the case. It is therefore proposed to calculate the η_i values associated with target μ_i at each floor of the MDOF EBF structure and then compute a weighted equivalent SDOF η value according to the work done at each level. This means that for values of μ_i less than one, Equation 2.10 is being implemented correctly and this is reflected in the equivalent SDOF η value. The equivalent SDOF η is therefore calculated as follows:

$$\eta = \frac{\sum_{i=1}^{n} V_i \theta_i \eta_i}{\sum_{i=1}^{n} V_i \theta_i}$$

Equation 2.19

where V_i and θ_i are the design storey shear and design interstorey drift at a given storey i, respectively.

2.3.5.4 *Design Base Shear and Lateral Force Distribution*

The design base shear obtained from Equation 2.12 is then distributed along the height of the structure in accordance with:

$$F_i = \begin{cases} k\dfrac{m_i \Delta_i}{\sum_{i=1}^{n} m_i \Delta_i} V_b & for \quad i < n \\[3em] (1-k)V_b + k\dfrac{m_i \Delta_i}{\sum_{i=1}^{n} m_i \Delta_i} V_b & for \quad i = n \end{cases}$$

Equation 2.20

where k is a term that is taken as 0.9 for structures with 6 or more storeys to account for higher mode effects as previously discussed in Section 2.3.5.2. This essentially takes 10% of the design base shear and places it at roof level to increase the design shear forces in the upper storeys and mitigate excessive drift amplification due to higher mode effects. The individual storey shears are then determined by summing all the lateral forces for each of the upper storeys as follows:

$$V_i = \sum_{j=i}^{n} F_j$$

Equation 2.21

2.3.6 Summary

To summarise the design procedure outlined in the previous sections, Figure 2.12 presents a flowchart of the steps involved in the DDBD of EBF structures with reference to each of the expressions proposed in the previous sections and providing further details about the DDBD process. A step-by-step example for the DDBD of EBFs has been provided in Sullivan [2013] for a 5-storey EBF building, and the reader is reminded that the proposals here supersede those of Sullivan [2013], but the general approach remains the same nonetheless, where the proposed modifications here give more confidence in the numerical modelling and determination of an appropriate DRF via an experimentally calibrated hysteresis model. The equations described above and in more detail in Sullivan [2013] can be easily implemented in a spreadsheet and thus the procedure is considered relatively simple. Nevertheless, it is also recognised that the DDBD procedure for EBFs does include considerably more steps than force-based alternatives such as the equivalent lateral force method. As such, future research could aim to simplify the procedure,

possibly in line with the proposals made by [Sullivan, 2013a] for the DDBD of RC frame buildings.
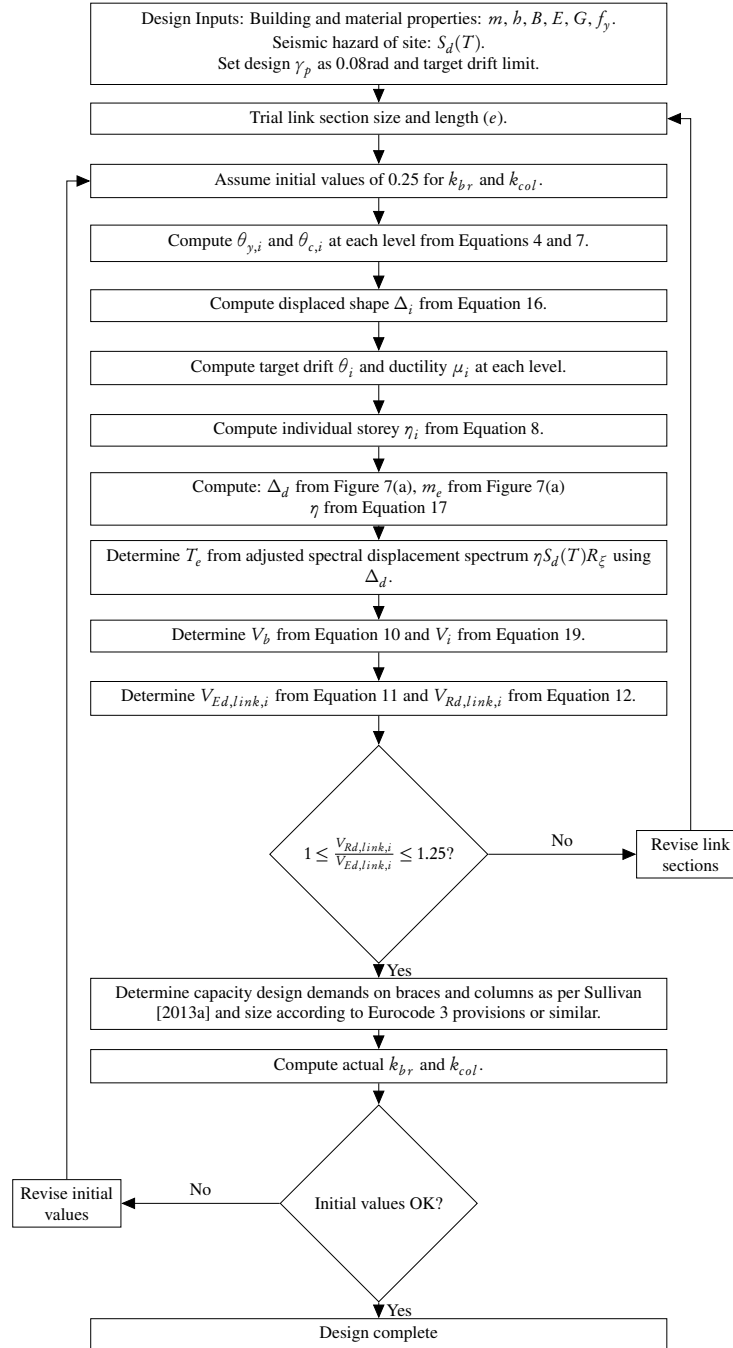
Figure 2.12: Flowchart for the DDBD of EBF structures.

2.4 DESIGN OF CASE STUDY BUILDINGS

In order to investigate the performance of the DDBD guidelines, a series of case study structures are designed using the proposed method. These structures vary in height from 1 to 15 storeys, and are also designed separately for two spectral shapes. The designs are then evaluated using NLTH analysis of the various structures to demonstrate the effectiveness of the method.

2.4.1 Description of Case Study Structure

2.4.1.1 *Structure Layout*

The case study structures examined in this study are shown in Figure 2.13, which consists of uniform bay widths of 7m in each direction and a uniform storey height of 3.5m. The variations of this structural configuration are structures with 1, 5, 10 and 15 storeys. In each case, the structure is assumed to have 4 EBFs as part of the lateral load resisting system in each direction. The seismic weights considered for the structure are noted in Figure 2.13 with each storey having a weight of 6,240kN, while the weight of the roof is taken as 5,500kN. European steel section sizes are used throughout and the grade of steel is chosen to be Grade 450 steel with nominal strength 450MPa, where the expected value of the material is taken as 528MPa in line with Badalassi *et al.* [2011], as DDBD requires actual material strength values to be used in place of nominal values. Sullivan *et al.* [2012] recommends that 1.1 times the nominal yield strength of steel may be used as the expected strength in the absence of more detailed material property information or material coupon test results.
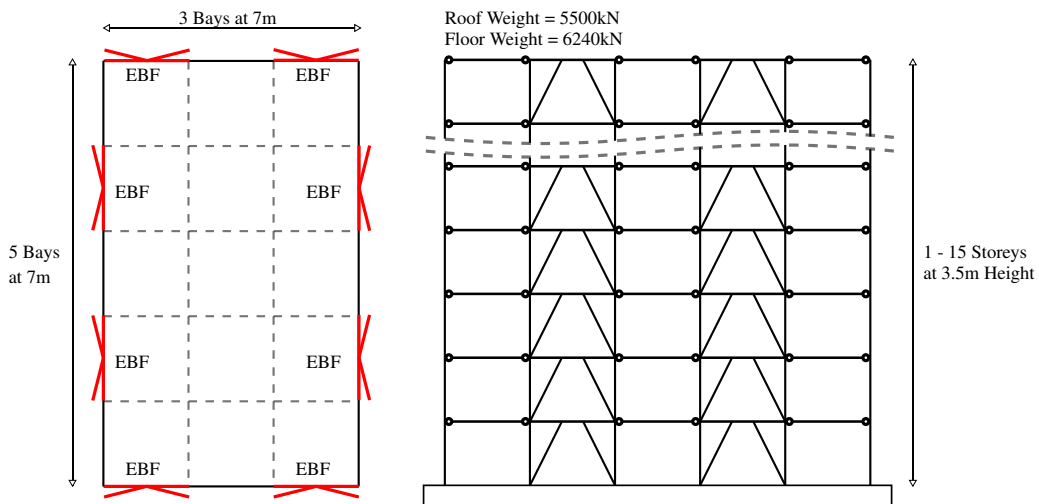
Figure 2.13: Plan and elevation layout of case study structure.

2.4.1.2   *Seismic Hazard*

The seismic hazard considered for the design of the case study structures consists of two different design spectra taken from Maley *et al.* [2013] and are shown in Figure 2.14. These spectra are EC8 type 1 spectra with soil type A and C, as per the soil type definitions outlined in EC8, modified such that both spectra have a spectral displacement corner period (T_D) of 8s. The reason for this long corner period, as opposed to 2s recommended by EC8, is that [Faccioli *et al.*, 2004] demonstrated that longer corner periods can be expected in certain regions of Italy (and elsewhere), and therefore the study by Maley *et al.* [2013] considered the effects of this in determining suitable design spectra. Both spectra have an equivalent peak ground acceleration (PGA) of 0.4g on hard rock, which means soil type A spectrum has a PGA of 0.4g whereas the soil type C has a slightly larger PGA due to soil effect amplification factors. These spectra shown in Figure 2.14 correspond to those used in the study by Maley *et al.* [2013] for which sets of ground motions were selected, scaled and are presented and discussed in Section 2.5.2.

| **(a) Design acceleration spectra** | **(b) Design displacement spectra** |
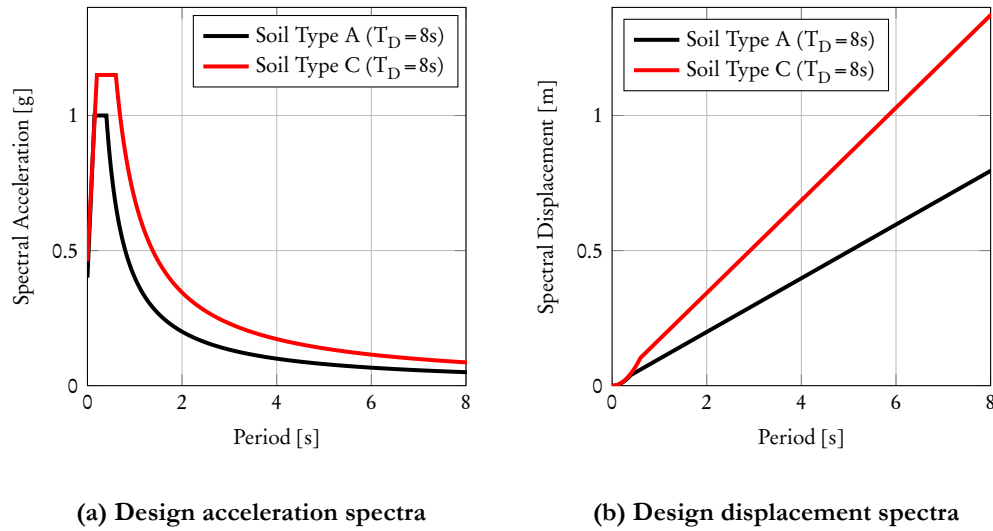
Figure 2.14: Design seismic hazard.

2.4.2   Design Criteria

The design criteria set out in this study are in accordance with the model code DBD12 [Sullivan *et al.*, 2012], where the interstorey drift limits of 2.5% are implemented to protect non-structural elements in addition to the plastic chord rotation limits of the links are set at 0.08 rad, although as will be seen in Section 2.4.3, the plastic chord rotation limits govern in each design scenario. For brevity, only peak interstorey drift and peak displacement are reported for each EBF design, along with the performance of the capacity design of the brace and column elements.

2.4.3 Case Study Designs

Each of the structure types considered were designed to both design spectra shown in Figure 2.14. Table 2.4 summarises the DDBD parameters used for the design of each structure in accordance with the procedure summarised in Figure 2.12, in addition to the total mass of structural steel required (M), as well as the final resulting base shear coefficient (C_s). For both of these parameters M and C_s reported in Table 2.4, it can be seen that the soil type C design requires more steel than that of soil type A, which is to be expected as the spectral ordinates were higher than soil type A in Figure 2.14. Similarly, the base shear coefficients C_s are much higher for the case of the soil type C design and tend to decrease with increasing number of storeys.

Table 2.4: DDBD Parameters.

Design Parameter		1 Storey	5 Storey	10 Storey	15 Storey
Soil Type A					
Δ_d	[m]	0.031	0.061	0.156	0.336
m_e	[T]	140.2	419.4	1341.3	1981.7
H_e	[m]	3.5	7.7	23.1	34.3
μ	[-]	3.4	2.36	1.71	1.26
η	[-]	0.588	0.662	0.812	0.858
T_e	[s]	0.48	0.84	1.72	3.52
M	[T]	108.2	426.1	3445	5295
V_b	[kN]	748.7	1440	2788.4	2309.1
Cs	[%]	54.4	32	18.1	9.9
Soil Type C					
Δ_d	[m]	0.042	0.094	0.296	0.39
m_e	[T]	140.2	422.6	1340.1	1987.2
H_e	[m]	3.5	7.7	23.1	34.3
μ	[-]	3.07	2.93	1.93	1.34
η	[-]	0.593	0.644	0.765	0.847
T_e	[s]	0.46	0.76	2.02	2.4
M	[T]	123.4	624.1	3885.4	8864.8
V_b	[kN]	1085.9	2706	3837.6	5316.4
Cs	[%]	79	60.2	24.9	22.9

From these structures designed using DDBD in Table 2.4, the resulting cross section member sizes for each design along with link length (e), design drift (θ_d), drift capacity (θ_c), storey design ductility demand (μ) and overstrength (Ω_{link}) of the provided to the required link strength are reported in Table 2.5 and Table 2.6 for both soil types A and C, respectively. It can be observed that as the number of storeys increases, the design ductility of the upper storeys reduces and the upper storeys are expected to respond elastically during seismic loading and hence, concentrate the inelastic behaviour in the lower storeys of the structure. This is a consequence of using the target displaced shape proposed in Equation 2.18, as the parabolic nature of the displaced shape means that the upper storeys are expected to be subjected to relatively little relative displacement and hence, interstorey drift in the first mode. In order to increase the target ductility in the upper storeys, the displaced shape could be adjusted to give a more linear shape. By doing this however, the contribution of higher modes of vibration may become more prominent and end up amplifying the interstorey drift in the upper and bottom storeys beyond the target design drift.

2.5 VERIFICATION ANALYSIS OF CASE STUDY BUILDINGS

In order to evaluate the DDBD method for EBF structures outlined in Section 2.3, the eight different structure typologies summarised in Table 2.5 and Table 2.6 evaluated through nonlinear time-history (NLTH) analyses using a series of spectrum compatible ground motion records for both design spectra. This section first discusses the additional numerical modelling parameters required for the dynamic analyses of the EBF structures, followed by the ground motion sets to be used for the NLTH analyses. The results of the NLTH analyses are then presented for each case to evaluate the DDBD methods robustness in the design of EBF structures.

Table 2.5: Soil Type A Design.

Storey	Level	Link	Brace	Column	e [m]	θ_d [%]	θ_c [%]	μ	Ω_{link}
1	1	HE200A	HE180B	HE160B	0.55	0.89	0.89	3.4	1.207
5	5	HE200A	HE160B	HE140B	0.5	0.39	1.15	0.68	1.191
	4	HE180B	HE200B	HE180B	0.6	0.57	1.28	0.96	1.037
	3	HE220B	HE200B	HE180M	0.8	0.75	1.5	1.28	1.075
	2	HE240B	HE220B	HE220M	0.8	0.93	1.37	2.05	1.083
	1	HE260B	HE240B	HE240M	0.8	1.11	1.22	3.57	1.138
10	10	HE450B	HE200B	HE180B	0.6	0.23	2.03	0.17	1.071
	9	HE500B	HE200B	HE200B	0.6	0.31	1.98	0.24	1.063
	8	HE500B	HE220B	HE240B	0.8	0.39	2.16	0.31	1.023
	7	HE500B	HE240B	HE280B	0.8	0.46	2.04	0.41	1.092
	6	HE450B	HE220M	HE340B	0.8	0.54	1.88	0.56	1.095
	5	HE400B	HE220M	HD360x196	0.8	0.62	1.77	0.72	1.072
	4	HE360B	HE220M	HD400x237	0.8	0.7	1.65	0.95	1.071
	3	HE360B	HE240M	HD400x262	0.8	0.77	1.46	1.41	1.103
	2	HE360B	HE240M	HD400x314	0.8	0.85	1.31	2.16	1.107
	1	HE360B	HE240M	HD400x382	0.8	0.93	1.16	3.81	1.131
15	15	HE360B	HE200B	HE160B	1.5	0.36	3.84	0.17	1.081
	14	HE400B	HE220B	HE180B	1.5	0.43	3.76	0.21	1.071
	13	HE450B	HE220B	HE200B	1.5	0.5	3.65	0.26	1.162
	12	HE450B	HE220B	HE360B	1.5	0.57	3.6	0.3	1.103
	11	HE450B	HE220B	HE300B	1.5	0.64	3.51	0.35	1.104
	10	HE450B	HE240B	HE320B	1.5	0.71	3.37	0.43	1.159
	9	HE400B	HE240B	HE400B	1.5	0.78	3.27	0.5	1.042
	8	HE400B	HE260B	HD400x237	1.5	0.85	3.16	0.59	1.115
	7	HE360B	HE280B	HD400x262	1.5	0.92	3.05	0.69	1.011
	6	HE340B	HE220M	HD400x287	1.4	0.98	2.77	0.85	1.059
	5	HE320B	HE220M	HD400x347	1.4	1.05	2.66	0.99	1.067
	4	HE320B	HE220M	HD400x382	1.4	1.12	2.53	1.21	1.057
	3	HE320B	HE220M	HD400x421	1.4	1.19	2.4	1.5	1.051
	2	HE320B	HE220M	HD400x463	1.4	1.26	2.26	1.92	1.056
	1	HE320B	HE220M	HD400x463	1.4	1.33	2.11	2.63	1.072

Table 2.6: Soil Type C designs.

Storey	Level	Link	Brace	Column	e [m]	θ_d [%]	θ_c [%]	μ	Ω_{link}
1	1	HE180B	HE200B	HE160B	0.7	1.19	1.19	3.07	1.031
	5	HE260B	HE220B	HE160B	0.8	0.48	1.69	0.62	1.082
	4	HE300B	HE240B	HE220B	1	0.73	1.9	0.96	1.052
5	3	HE340B	HE300B	HE240M	1	0.97	1.78	1.54	1.013
	2	HE400B	HE300B	HE260M	1	1.22	1.66	2.37	1.167
	1	HE400B	HE300B	HE300M	1	1.46	1.51	3.95	1.128
	10	HE400B	HE200B	HE160B	1.2	0.45	3.01	0.28	1.063
	9	HE450B	HE220B	HE220B	1.2	0.6	2.93	0.38	1.078
	8	HE450B	HE240B	HE280B	1.4	0.74	3.12	0.49	1.011
	7	HE450B	HE260B	HE340B	1.5	0.89	3.16	0.62	1.028
	6	HE450B	HE220M	HE450B	1.5	1.03	3	0.8	1.138
10	5	HE400B	HE240M	HD400x237	1.5	1.18	2.85	1.03	1.081
	4	HE400B	HE240M	HD400x287	1.5	1.32	2.7	1.34	1.019
	3	HE450B	HE240M	HD400x347	1.5	1.46	2.52	1.81	1.152
	2	HE450B	HE240M	HD400x421	1.5	1.61	2.36	2.48	1.138
	1	HE450B	HE260M	HD400x509	1.5	1.75	2.19	3.68	1.15
	15	HE500M	HE180M	HE200B	1.7	0.38	4.53	0.15	1.022
	14	HE600M	HE200M	HE240B	1.7	0.47	4.42	0.19	1.025
	13	HE650M	HE200M	HE260B	1.7	0.55	4.3	0.24	1.037
	12	HE650M	HE220M	HE340B	1.7	0.64	4.16	0.29	1.028
	11	HE650M	HE220M	HD400x262	1.7	0.72	4.08	0.34	1.024
	10	HE650M	HE240M	HD400x287	1.7	0.81	3.93	0.41	1.074
	9	HE600M	HE240M	HD400x314	1.7	0.89	3.81	0.48	1.05
15	8	HE550M	HE240M	HD400x347	1.7	0.98	3.67	0.57	1.044
	7	HE500M	HE240M	HD400x421	1.7	1.06	3.54	0.67	1.043
	6	HE600B	HE240M	HD400x509	1.7	1.15	3.33	0.83	1.026
	5	HE550B	HE260M	HD400x551	1.7	1.23	3.17	1.01	1.047
	4	HE550B	HE260M	HD400x634	1.7	1.32	2.99	1.25	1.033
	3	HE550B	HE260M	HD400x744	1.7	1.4	2.82	1.59	1.027
	2	HE550B	HE260M	HD400x818	1.7	1.49	2.65	2.09	1.032
	1	HE550B	HE260M	HD400x900	1.7	1.57	2.48	2.92	1.047

2.5.1 Dynamic Analysis Modelling Parameters

A 2D model consisting of force-based fibre elements is developed in OpenSees [McKenna *et al.*, 2000] for the design verification using the EBF link numerical modelling procedure outlined in Section 2.2.2.1. For the beam and column elements, force-based fibre elements with 7 integration points per element are used for these members with the Giuffre Menegotto-Pinto material model. A total of 20 fibres are used along both the web depth and flange width of sections, while 5 fibres are used along the thickness. Second order geometry effects (P-Delta) are modelled through the use of a dummy column outside of the structure, which is pinned at each floor level to model the gravity loading of the structure not attributed directly to the EBF frame being modelled. Since the case study structure is symmetric in both directions, significant torsional response is not anticipated and only one EBF is modelled with one quarter of the tributary mass and loads are assigned to this frame. The masses are therefore lumped at each floor at each of the exterior column nodes, which are also pinned at the base connection. A Newmark integration scheme was adopted with a time step of 0.001s. For the elastic damping model, 3% Rayleigh tangent stiffness proportional damping is assigned to the first and third modes of vibration of the structures. The lateral resistance of the internal gravity system is assumed to be negligible and is not modelled.

2.5.2 Ground Motion Sets

As mentioned previously in Section 2.4.1.2, the design spectra used in this study consist of those used in a similar study by Maley *et al.* [2013]. In that study, a series of ground motion sets were selected in order to conduct NLTH verification analysis and are used here and the individual spectra for each set along with their respective means are shown in Figure 2.15 for both spectral acceleration and spectral displacement.

2.5.3 Analysis Results

The following sections plot the peak interstorey drift and peak displacement for each of the case study structures designed to the different design spectra. The design drift and displaced shape are plotted with the individual ground motion responses and mean of these ground motions to evaluate the performance of the DDBD method for each of the designs considered.
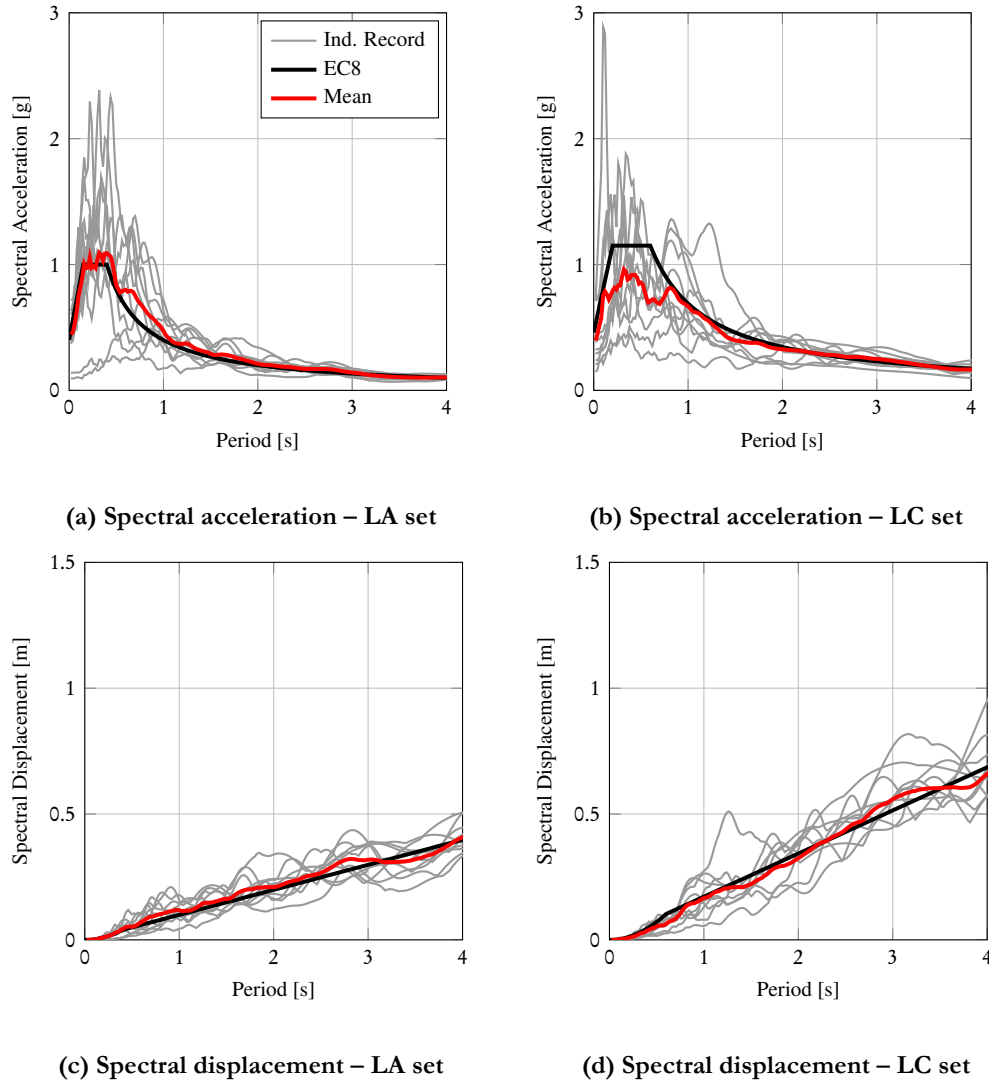
(a) Spectral acceleration – LA set

(b) Spectral acceleration – LC set

(c) Spectral displacement – LA set

(d) Spectral displacement – LC set

Figure 2.15: Response spectra of compatible ground motions from [Maley *et al.*, 2013].

2.5.3.1   *Interstorey Drift*

Figure 2.16 shows the interstorey drift profiles for the case study structures. It can be seen that the DDBD method has worked very well in controlling the interstorey drift of the EBF structures for each of the case study buildings. Note that for the single storey EBFs in Figure 2.16(a) and Figure 2.16(e), the link capacity drift (θ_c) and design drift (θ_d) correspond to the same storey drift as per Table 2.5 and Table 2.6 and hence, only the line for θ_c is visible in the plots. However, the response to soil type A ground motions

appears to be a lot closer to the link capacity than that of the soil type C responses. Part of the reason could be greater higher mode effects that result for this spectral shape (see Roldan *et al.* [2014], Nievas and Sullivan [2015]). In general, the results obtained are encouraging. The design drift profile set out in DDBD has ensured that the interstorey drift does not exceed the link capacity in all cases. In addition to this, the design profile has limited the interstorey drift contributions of the higher modes of vibration. For example, the interstorey drifts observed in the 15 storey building in Figure 2.16(h) show a slight increase in the drift of the upper floors due to the second mode of vibration's contribution. However, the design displacement profile has been set out in such a way in Section 2.3.5.1 that this increase in interstorey drift in the upper floors appears to be adequately controlled. The exceedance of the design interstorey drift profile in lower floors of Figure 2.16(d) is also deemed acceptable as despite this exceedance, the proposed displaced shape was reduced to allow for higher mode drift amplification to be considered such that the modal combination does not exceed the link capacity at any level, as illustrated in Figure 2.11. Comparing with Sullivan [2013], drift concentrations for the case of the 15 storey structure are not observed here due to the careful control of link overstrength ratio (Ω_{link}) and the overstrength gradient between levels. A limit of 1.25 was proposed here, where looking at the values Table 2.5 and Table 2.6, this limit is well respected and is reflected in the results shown in Figure 2.16.

2.5.3.2   *Displacement*

Figure 2.17 shows the maximum displacement response of each of the case study structures examined. As can be seen for each of the cases, the displaced shape of the EBF's remains quite close to that of the target design displacement except over the upper storeys of the structure which adopt a relatively linear profile. This is attributed to the higher mode reduction factors applied to the displaced shape to prevent excessive drift amplification and also the elastic behaviour anticipated in the upper storeys, as seen in Table 2.5 and Table 2.6. Ideally, the section sizes in the upper storeys of the taller structures may be sized an a way that would encourage more ductile behaviour, as from Figure 2.16 there is still a lot of drift capacity available before link capacities would begin to be exceeded. One possibility could be to revise the lateral load distribution from that proposed in Equation 2.20 to an approach similar to that proposed by Roldan *et al.* [2014] for MRF structures showing quite positive results. This approach allows more flexibility in the design storey shear distribution while at the same time providing the required base overturning moment as required by the DDBD procedure, although this is a refinement beyond the scope of this paper.
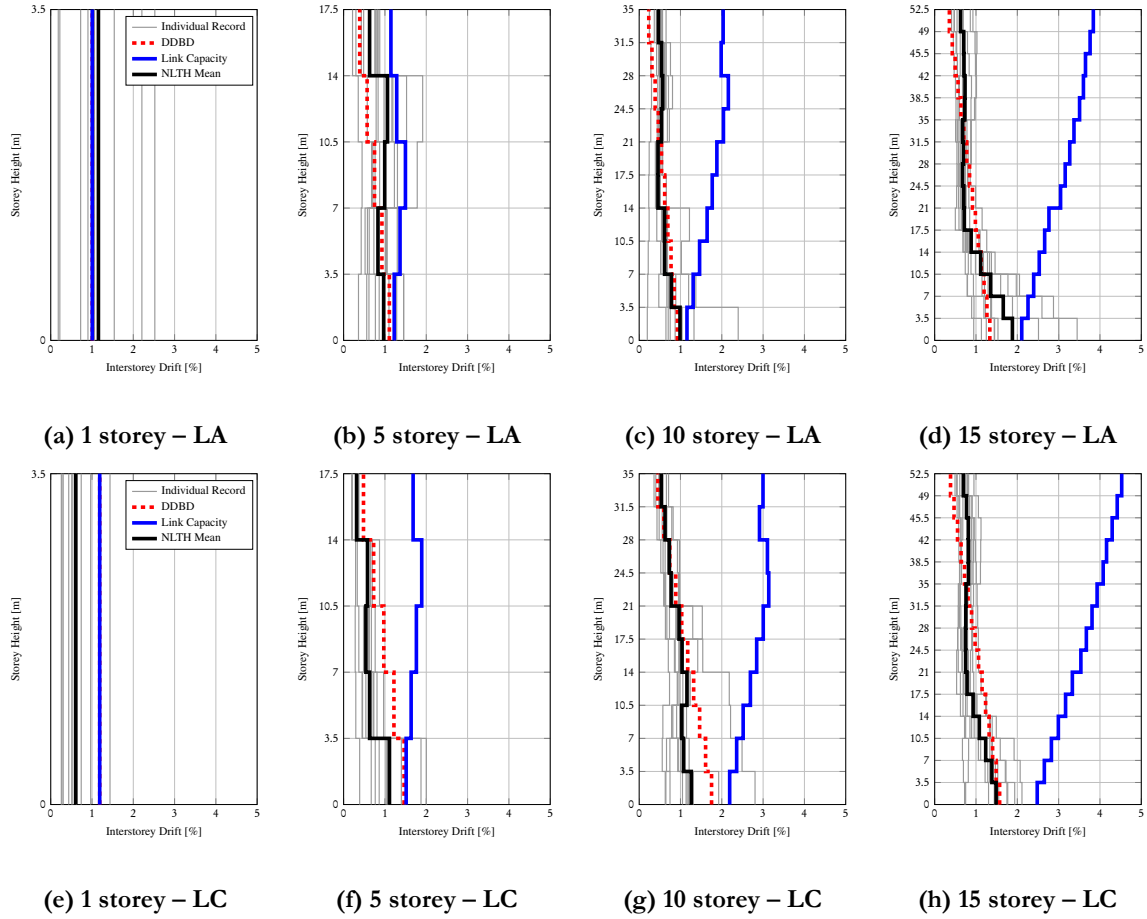
(a) 1 storey – LA   (b) 5 storey – LA   (c) 10 storey – LA   (d) 15 storey – LA

(e) 1 storey – LC   (f) 5 storey – LC   (g) 10 storey – LC   (h) 15 storey – LC

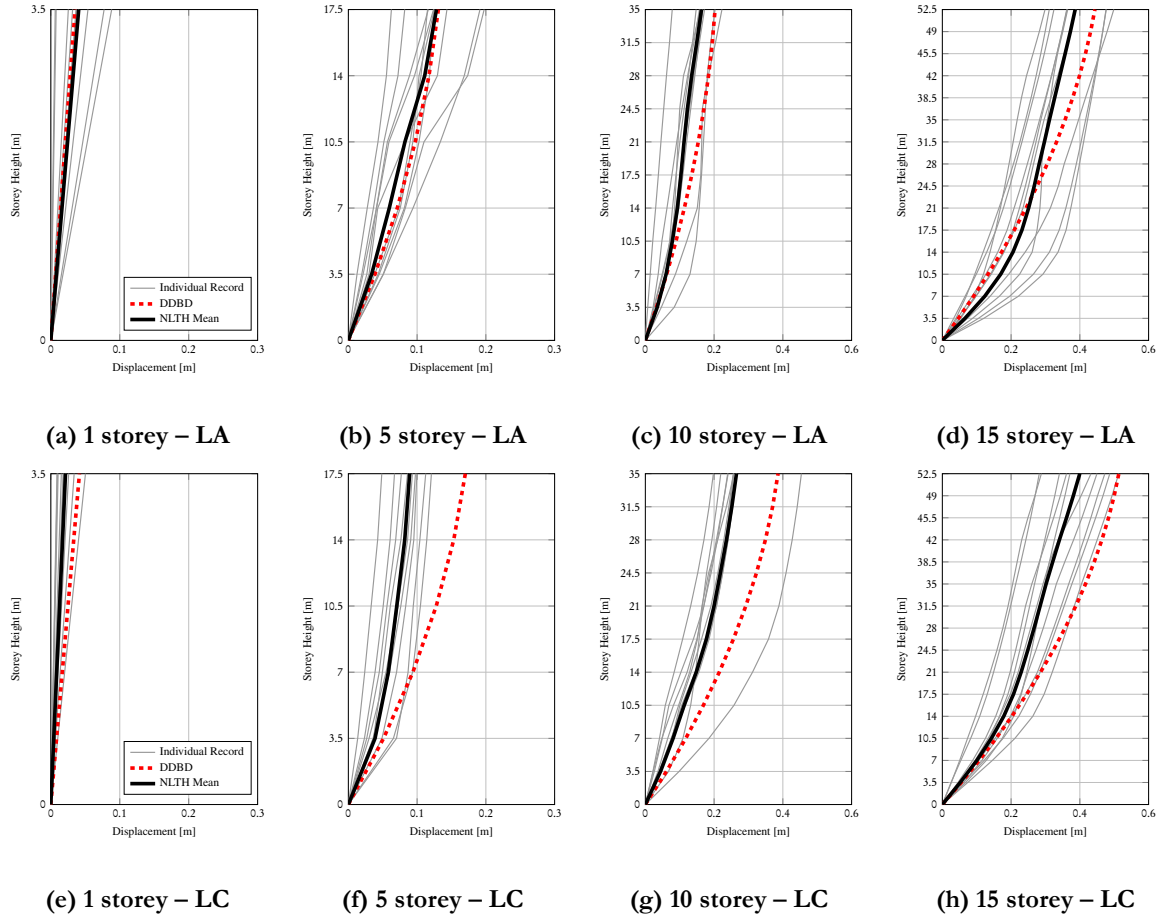Figure 2.16: Interstorey drift response for both ground motion sets.

Figure 2.17: Displacement response for both ground motion sets.

2.5.3.3 *Beam and Column Capacity Design*

In terms of the capacity design of the brace and column elements outlined in Section 2.3.2.5, a comparison between the observed and provided axial force capacities is provided in Figure 2.18, which plots the ratio of the observed mean axial force from NLTH analyses as a ratio to the member capacities. These are plotted versus the normalised height of each of the case study structures, where the terms in the legend, such as 5-A, indicates the 5 storey structure designed for soil type A. Figure 2.18 shows that the demand to capacity ratios are less than unity in all cases for both braces and columns, demonstrating the effectiveness of the capacity design provisions outlined in Section 2.3.2.5. Another observation is the slight decrease in the demand to capacity ratio, especially in the case of the 15 storey structure designed using the soil type A spectrum. This can be explained by the capacity design assumption that a full mechanism would

form over the height of the EBF, which is a worst-case scenario that is not very likely. This is recognised in some codes (e.g. [AISC 341-10, 2010; CSA S16-09, 2009; NZS 3404, 2007]), where a reduction in the amplification of column axial loads is permitted for high rise structures to take this into account. However, since there is no obvious and clear trend in Figure 2.18 that would suggest a relaxation of capacity design amplification factors for columns in tall EBF structures, no reduction in amplification is suggested here. However, further studies could be conducted to provide more insight on this subject, not only for EBFs but for frame structures in general.
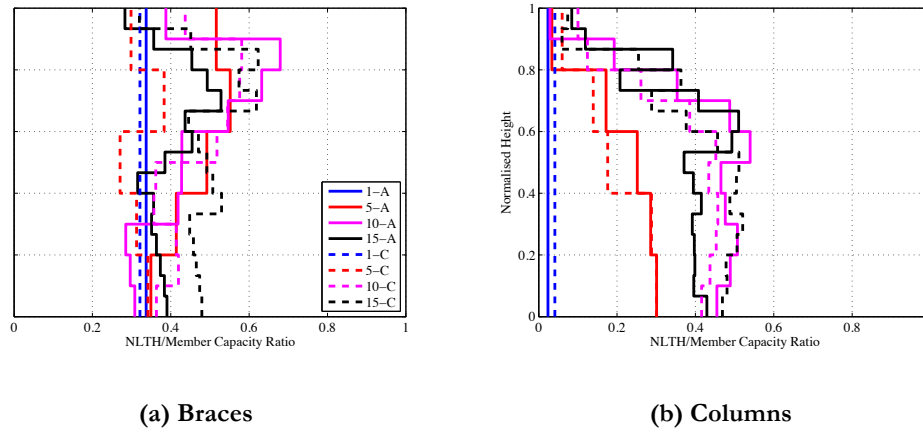

(a) Braces   (b) Columns

Figure 2.18: Ratio of NLTH axial force to axial force capacity for each design case.

2.6 SUMMARY

This paper has developed and verified tools for the DDBD of eccentrically braced steel frame structures. A review into current design code approaches to the design of a series of SDOF EBFs was carried out to illustrate an important clarification required in Eurocode 8 for the determination of plastic link demands when using elastic analysis for design. In addition, these design case studies showed that current force-based methods do not provide a direct method to control design deformation demands which then provided motivation for a displacement-based design approach for EBFs. The design method was discussed to present and justify the various steps used in the design procedure. Among these, important refinements include the calibration of a spectral displacement reduction factor to relate the displacement of the inelastic system to that of the equivalent linear system used in DDBD. This was developed using the experimentally calibrated link element model that more accurately represents the behaviour of EBF links compared to more simplified bilinear hysteresis models that do not account for isotropic hardening in the links. The complete method was then summarised into a step-by-step flow chart in Figure 2.12, and a series of case study structures were designed. These included four structure types ranging from a single storey to a 15 storey structure,

designed for two different spectral shapes. Nonlinear time-history analyses were then used to evaluate each of these design case study structures and the results of the analysis were compared in terms of the control of interstorey drift, displaced shape and also the capacity design of the brace and column members.

3. FRAGILITY FUNCTIONS FOR ECCENTRICALLY BRACED STEEL FRAMES

This chapter is based on work published in O'Reilly and Sullivan [2016], available at:

O'Reilly, G. J., Sullivan, T. J. [2016] "Fragility Function for Eccentrically Braced Frame Structures," *Earthquakes and Structures*, (Accepted for Publication).

3.1 INTRODUCTION

Seismic assessment of structures in terms of economic loss and downtime typically aims to relate the probability of a certain damage state with the seismic response of the structure through the use of fragility functions. These damage states can then be related to a cost of repair for that damage state and an associated repair time to give an estimation of the structure's economic loss and downtime. Fragility functions for different types of structures may be determined based on experimental testing, numerical analyses or by engineering judgement in the absence of test data [FEMA P58-1, 2012].

For eccentrically braced frame (EBF) structures, such as that shown in Figure 3.1, Gulec *et al.* [2011] report test data from 110 different experimental tests on EBF links available in the literature and compile a database relating the occurrence of different damage limit-states to a plastic chord rotation, which was chosen as the engineering demand parameter (EDP). However, since the link plastic chord rotation is a demand parameter not typically utilised in current assessment software, such as the Performance Assessment Calculation Tool (PACT) software [FEMA P58-1, 2012; FEMA P58-2, 2012], this set of fragility functions for EBFs creates difficulty in terms of its ease of application. Typically, EDP's such as interstorey drift and floor accelerations are used when performing a seismic assessment using software tools such as PACT, which represents the current state-of-the art in seismic assessment. As such, the goal of this paper is to develop a set of fragility functions for EBFs, which are based on interstorey drift as opposed to link plastic chord rotation, which can be quite tedious to establish whereas interstorey drift is a parameter engineers are more familiar with and already use in seismic assessment. From this, the user will be able to use a set of fragility functions for EBF structures in terms of the more familiar EDP interstorey drift, in addition to doing away with the need to separate the link demand in terms of its elastic and plastic components. It will be also shown by using the approach outlined here, a set of fragility functions can be derived for an EBF structure with just information about structural geometry, given certain simplifications.

This latter approach represents a useful tool when conducting a more general and regional assessment of EBF structures.

This paper first examines the behaviour of EBFs by reviewing the expressions needed to calculate the yield interstorey drift of a single storey within an EBF system. Advanced numerical analyses are then used to illustrate the validity of the yield drift expression. Existing EBF fragility curves are discussed and the basis for the development of the interstorey drift-dependant fragility functions is then presented. This paper finally presents the analysis results and proposed fragility functions and demonstrates the application of each of these through example.
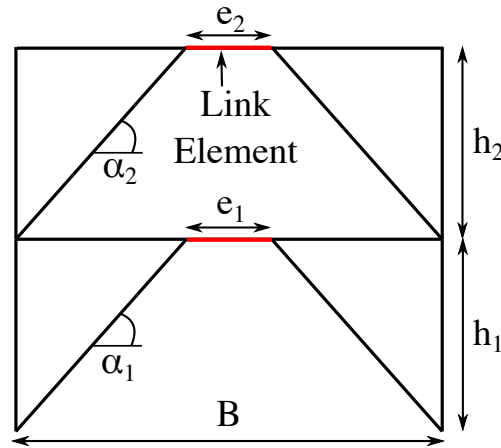

Figure 3.1: Typical layout of an EBF.

3.2 CHARACTERISING THE BEHAVIOUR OF ECCENTRICALLY BRACED FRAME STRUCTURES

EBF structures resist intense seismic loading through the inelastic deformation of a link element, such as that shown in Figure 3.1, which can be classified as either a short or long link through the ratio ρ, which is defined as:

$$\rho = \frac{e}{M_p / V_p}$$ **Equation 3.1**

where e is the link length as per Figure 3.1, M_p and V_p are the plastic moment and shear capacities of the link section, respectively. A ρ value of 1.6 or less indicate a short link which yields primarily in shear as defined in numerous design codes such as AISC 341-10, CSA S16-09, Eurocode 8 and NZS 3404, whereas a ρ value greater than 3.0 indicates a

long link which yields primarily in flexure, according the European and New Zealand standard, whereas the US and Canadian standards define a slightly lower value of 2.6. Link with values of ρ between these limits are expected to develop a combined flexure shear response.

In order to relate the interstorey drift demand with the likelihood of exceeding a certain damage state in an EBF structure, one requires expressions for both the elastic (yield) interstorey drift and plastic interstorey drift capacity, which summed together to give the total interstorey drift capacity. This section first presents an expression for the yield drift of EBF systems proposed by Sullivan [2013b] which is reviewed and existing relationships for the plastic drift capacity relating the link chord rotation demand to the interstorey drift demand are combined to arrive at an estimate of the total drift capacity.

3.2.1 EBF Yield Drift Expression

As explained in Sullivan [2013b], the yield drift of an EBF structure is principally composed of three deformation components:

- Beam (including link) bending and shear deformation.
- Brace axial deformation.
- Column axial deformation.

This section presents simplified expressions to calculate each of these three components and in turn, the yield drift of an individual storey in an EBF structure consisting of a single bay with a single central link element, as illustrated in Figure 3.1. This yield drift relationship is then compared to values obtained from an experimentally validated numerical model of various configurations of an EBF structure.

3.2.1.1 *Beam Deformation Component*

An expression to describe the vertical displacement of a single beam section at the end of each link due to vertical shear forces developed in the link during loading is described in Mazzolani *et al.*, [2006] and is elaborated in Sullivan [2013b] to give an expression which gives the interstorey drift at the point of yielding in the links. One of the assumptions is that the beam cross-section remains the same for regions both outside and within the link section of the beam. This implies that in order to use systems such as those discussed in Mansour [2010], which may comprise of removable links with different cross sections to the surrounding beam elements, the following expressions would need to be adjusted. The resulting expression for the drift contribution due to link deformation of a given storey i, depicted in Figure 3.2(a), is given in Sullivan [2013b] by:

$$\theta_{link,i} = \frac{f_y A_{v,i} e_i}{\sqrt{3}(B - e_i)} \left(\frac{e_i(B - e_i)}{12EI_{zz,i}} + \frac{1}{GA_{v,i}} \right) \qquad \text{Equation 3.2}$$

where the general notation is as illustrated in Figure 3.2(a), with I_{zz} representing the second moment of area of the beam about the major axis, f_y is the steel yield strength, E and G are the elastic and shear moduli of steel, respectively. The shear area (A_v) is taken to be the product of the entire height of the section (h) times the web thickness (t_w) as recommended by Della Corte *et al.* [2013], which concluded that this represents the best estimate of shear area of European HE link sections compared to the expression given in Eurocode 3 [EN 1993-1-1:2005, 2005] when comparing the shear stiffness of both expressions to values obtained from finite element analyses.

3.2.1.2   *Brace Deformation Component*

The expression describing the deformation contribution due to the axial elongation of the brace elements depicted in Figure 3.2(b) is given in Sullivan [2013b] as:

$$\theta_{br,i} = \frac{2k_{br,i}\varepsilon_y}{\sin(2\alpha_i)} \qquad \text{Equation 3.3}$$

where ε_y is steel yield strain, α is the brace angle and $k_{br,i}$ represents the brace strain ratio, which can be computed as the ratio of the seismic design axial force, $N_{Ed,br,i}$, to the brace section yield force, $N_{c,Rd,br,i}$:

$$k_{br,i} = \frac{N_{Ed,br,i}}{N_{c,Rd,br,i}} \qquad \text{Equation 3.4}$$

where the terms $N_{Ed,br}$ and $N_{c,Rd,br}$ represent the design action and capacity axial forces of the brace section, respectively, where the axial capacity is the full section compression capacity (i.e. Af_y) and is not to be confused with the buckling capacity of the member. The product of $k_{br,i}$ with ε_y gives the expected axial strain in the brace at yield of the link and therefore, knowing the brace strain and length, the brace contribution to the interstorey drift can be found.
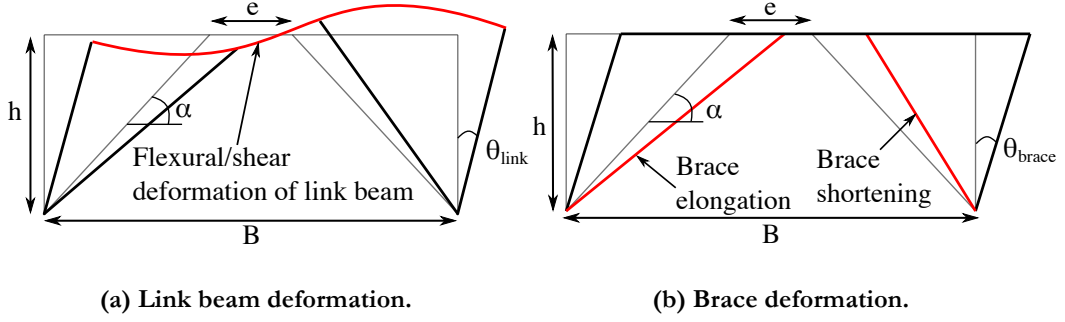
(a) Link beam deformation.   (b) Brace deformation.

Figure 3.2: Link and brace deformation components.

3.2.1.3 *Column Deformation Component*

For a given storey in a multi-storey building, the axial deformations of the columns in the lower storeys lead to the development of a rigid body rotation of the storeys above. This contribution is calculated in much the same way as the brace elongation contribution, where the ratio of the design force to the section yield force is used to provide an estimate of the expected column strain, which can then be converted into an equivalent rigid body rotation of the storey, as depicted in Figure 3.3(a). This is given by:

$$\theta_{col,i} = \frac{2k_{col,i-1}\varepsilon_y H_{i-1}}{B}$$

Equation 3.5

where H_{i-1} is the elevation of the floor below the one being considered and $k_{col,i-1}$ represents the average column strain ratio. As there can be many storeys below the storey i being considered, there are many ratios of design to capacity axial load ratios. The average value of these is therefore used in the expression, which is thus calculated by:

$$k_{col,i-1} = \frac{1}{i-1}\sum_{j=1}^{i-1}\frac{N_{Ed,col,j}}{N_{c,Rd,col,j}}$$

Equation 3.6

where $N_{Ed,col}$ represents the design axial force on the column member and $N_{c,Rd,col}$ the full compressive capacity of the column section, again not to be confused with the member buckling capacity.

In addition to the axial deformations of the storeys below the one being considered, there is also the contribution of the axial deformations of the storey in question, which is shown in Figure 3.3(b). The contribution of this deformation mode is noted in Sullivan (2013), where it was proposed to simply ignore it, as it is difficult to incorporate into the expression in Equation 3.7, and also because the exclusion of this term gave reasonably

accurate results in any case. For a given storey, this additional deformation due to the axial elongation and shortening of the storey's column is derived as follows:

$$\theta_{col,axial,i} = \frac{1}{h_i}\sqrt{\left(\frac{B-e_i}{2}\right)^2 + h_i^2 - \left(h_i - \frac{\overline{V}_i e_i h_i}{BEA_{col,i}}\right)^2} - \frac{1}{\tan\alpha_i} \qquad \textbf{Equation 3.7}$$

where h_i is the individual storey height and $A_{col,i}$ is the cross-sectional area of the column.

(a) Rigid body rotation of storey.   **(b) Column axial deformation.**
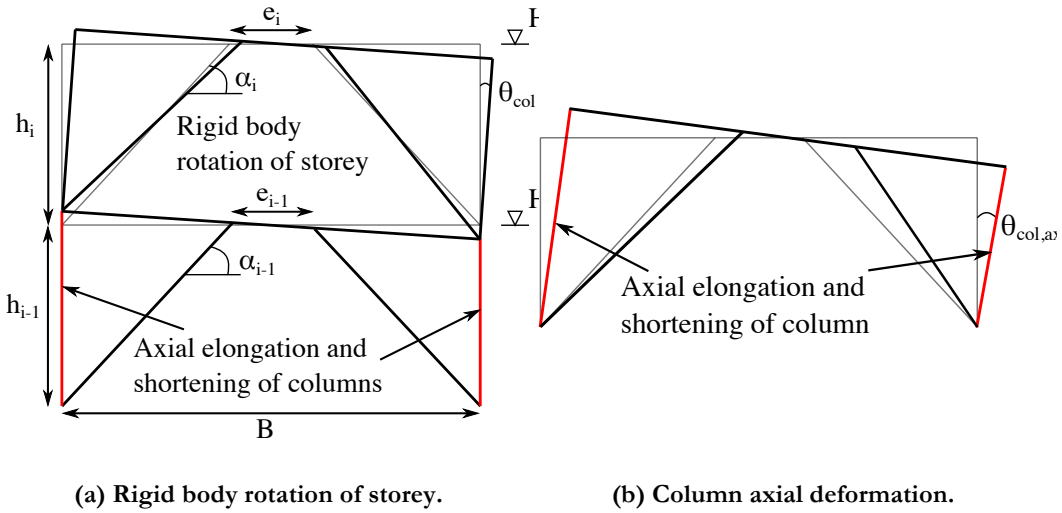
Figure 3.3: Column deformation components.

Figure 3.4 shows the relative contributions of each of the link deformation, brace deformation, rigid body rotation due to axial deformations of lower columns and the drift contribution due to the axial deformations of the given storey for a variety of EBF structures. These yield drift contributions represent the yield drift contributions at the roof level of each of the soil type C designs outlined in O'Reilly and Sullivan [2015] which consisted of uniform storey heights of 3.5m, bay width of 7m and S450 grade steel. These structures were all designed to a Eurocode 8 [EN 1998-1:2004, 2004] response spectrum for a soil type C site which has an equivalent PGA on soil type A of 0.4g. It can be seen from Figure 3.4 that the relative contribution of the column's axial deformations is quite small (less than 2% of the total yield drift), which confirms the remarks by Sullivan [2013b] that it has relatively little contribution to the overall interstorey drift and can be ignored, given its lengthy expression.

Combining the above expressions for the links, braces and columns, the total storey drift at yield of a single storey within an EBF structure can be computed:

$$\theta_{y,i} = \theta_{link,i} + \theta_{br,i} + \theta_{col,i}$$

Equation 3.8

$$= \frac{\overline{V}_i e_i}{B - e_i} \left(\frac{e_i(B - e_i)}{12EI_{zz,i}} + \frac{1}{GA_{v,i}} \right) + \frac{2k_{br,i}\varepsilon_y}{\sin(2\alpha_i)} + \frac{2k_{col,i-1}\varepsilon_y H_{i-1}}{B}$$

(a) 1 Storey

(b) 5 Storey
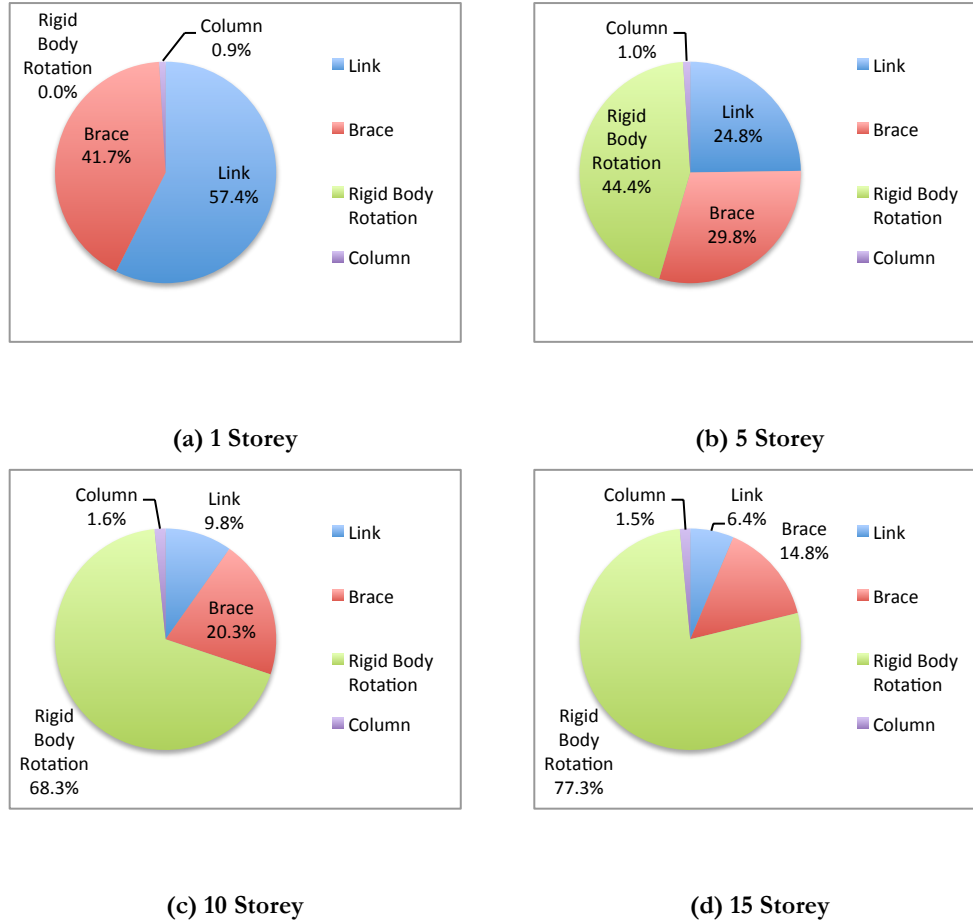

(c) 10 Storey

(d) 15 Storey

Figure 3.4: Yield drift contribution of each of the deformation components.

3.2.2 Verification of Yield Drift Expression for EBFs

The yield drift expression given by Equation 3.8 can be compared with results obtained from a numerical model to gauge its accuracy and validate its use later in this study. Hence, the validation of expressions describing the yield drift of a range of EBFs is required to proceed with confidence. A total of 112 variations of the EBF model were analysed from pushover analysis using OpenSees [McKenna *et al.*, 2000]. The variations consisted of EBFs with a constant storey height of 3.5m, bay width of 7M and grade S355 steel. Section sizes were varied between HE160B and HE650M of the European section size catalogue [Corus, 2006], where for each section size, the link length was determined as 40, 50 and 60% of the maximum link length in order to remain classified as a link length, which is found by rearranging the expression in Equation 3.1. The model, illustrated in Figure 3.5, consists of a force-based beam-column element for the modelling of the link elements in axial and flexural behaviour with an uncoupled shear hinge added to the link element to model the nonlinear shear behaviour expected in short links. Brace elements have been modelled as elastic truss elements with pinned end connections. Column members have also been modelled as elastic elements as these, along with the braces, are expected to remain elastic throughout nonlinear response. In addition, the connection between the beams and the columns is modelled as a pinned connection, as shown in Figure 3.5. In addition, a comparison between the link shear behaviour predicted by the proposed OpenSees model with a specimen tested by Mansour [2010] is also shown in Figure 3.5, where an excellent match between the numerical model and the experimental response both in terms of the link capacity and hysteretic behaviour can be observed. Since the purpose of using such a model in this study is to evaluate the expression derived for the yield drift of the EBF configuration, no fracture criterion has been considered, although such a model may be adopted in the future to include such considerations either by introduction of an upper limit on the deformation capacity through the use the MaxMin material model available in OpenSees, or through the introduction low-cycle fatigue similar to that developed by Uriz and Mahin [2008] for concentrically braced steel frames by utilising experimental testing and observations by Okazaki et al. [2005] for example, but such work is deemed beyond the scope of this paper. Further detailing on the modelling and its calibration can be found in the original publication by O'Reilly and Sullivan [2015].
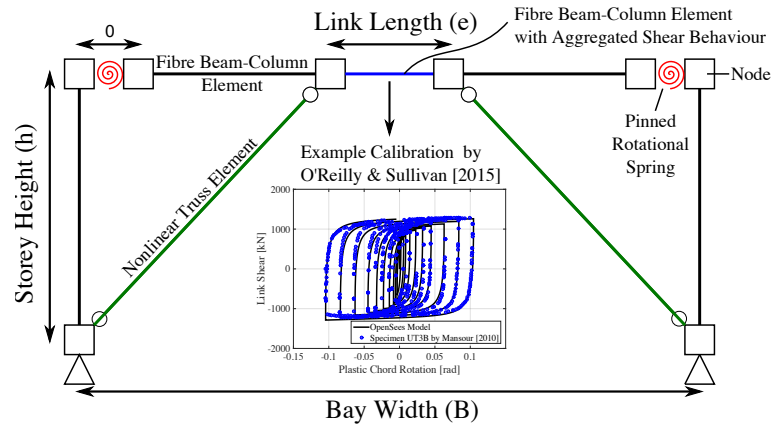
Figure 3.5: Illustration of EBF model proposed by O'Reilly and Sullivan [2015].

From these pushover analyses performed on existing designs of EBFs, the yield drift was determined and compared to what is given by Equation 3.8 in each case. A comparison of these two sets of data is shown in Figure 3.6, where the predicted yield drift is plotted against the observed numerical drift. As is evident from Figure 3.6, Equation 3.8 predicts the yield drifts well and is deemed to be sufficient for later use in conjunction with an expression for plastic drift to give the total drift capacity of a single storey, which is discussed further in Sections 3.2.4 and 3.2.5.

Figure 3.6: Predicted versus observed yield drift.

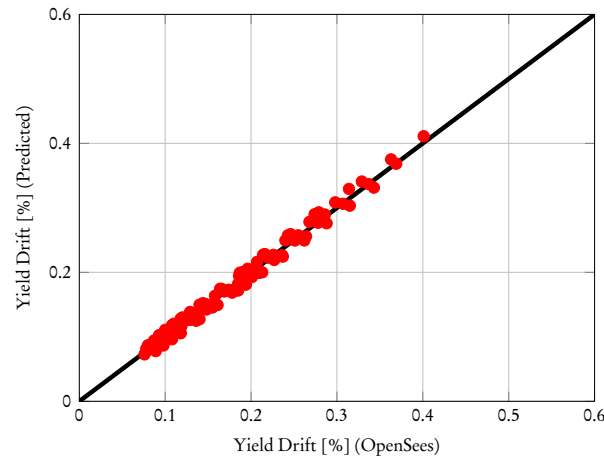### 3.2.3 EBF Yield Drift Parameter Sensitivity

The expression developed for the yield drift of an EBF in Section 3.2.1 consists of a number of terms relating to the geometry and member properties of an EBF. In order to evaluate the sensitivity of the yield drift to these individual parameters, a parametric study is conducted in order to establish the principle parameters that contribute to the variation of yield drift for a given reference configuration. This reference configuration is taken as a HE280B section for links and columns with a 600mm link length at the fifth storey in a structure. The brace and column strain ratios (Equation 3.4 & Equation 3.6) are taken as 0.3 and 0.4, respectively, which are deemed reasonable values noting that the ratio is usually significantly less than 1.0 as a result of differences between member buckling and resistance and the section resistance used in Equation 3.4 & Equation 3.6. The values varied in this study are given in Table 3.1 together with the relevant justifications, which are based on engineering judgement.

Table 3.1: Sensitivity study parameter range.

Parameter		Range	Step	Unit	Justification
Link length	e	300-1400	100	mm	Upper limit in order to maintain $\rho < 1.6$
Bay width	B	5-12	0.5	m	Reasonable range of bay widths.
Storey height	h	3-5	0.5	m	Reasonable range of storey heights.
Number of storeys	n	1-10	1	-	Reasonable range of storeys.
Link shear area	A_v	640-6750	-	mm^2	HE140B to HE550A section sizes.
Yield strength	f_y	235-450	-	MPa	Grades S235, S275, S355 and S450 steel.

Computing the yield drift from Equation 3.8 for the range of parameters listed in Table 3.1 which are normalised by the reference configuration described above, the influence of different parameters on the yield drift normalised by the yield drift of the reference configuration are given in Figure 3.7, where it can be seen that the influence on yield drift varies greatly between parameters. It can be seen that the parameters that the yield drift is most sensitive to are the number of storeys, where the elastic rigid body rotation of the storeys below increases as the number of storeys increases, steel yield strength and bay width. In addition to these, it can be seen that the storey height has minimal influence on the yield drift of the storey, hence it is deemed to be insensitive to these parameters and this is not considered in the drift capacity fragility analysis discussed in Section 3.3.
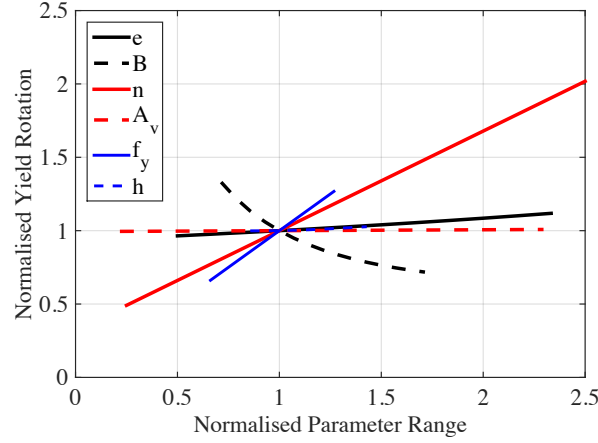
Figure 3.7: Normalised yield drift sensitivity.

3.2.4 EBF Plastic Drift Capacity

Experimental testing by Engelhardt and Popov [1989a] at the University of California, Berkeley in the 1980's reported the deformation capacity of the links in terms of the plastic chord rotation (γ_p), where the elastic component rotation was removed. For short links, Engelhardt and Popov [1989a] proposed 0.08rad for the design plastic rotation of short links, which were defined as the deformations for which a well-detailed link was able to provide stable hysteresis. These design limits for plastic chord rotation appear to have been subsequently adopted in design codes such as Eurocode 8 [EN 1998-1:2004, 2004], AISC 341-10 [AISC 341-10, 2010], CSA S16-09 [CSA S16-09, 2009] and NZS 3404 [NZS 3404, 2007].

In order to define the plastic storey drift capacity, these limits need to be related to an interstorey drift, which is given by:

$$\theta_{p,i} = \frac{e_i \gamma_p}{B}$$

Equation 3.9

In addition to the experimental data from Engelhardt and Popov [1989a], which appears to have been subsequently adopted by most design codes, Gulec *et al.* [2011] collects data from 110 different tests, including more recent testing at the University of Texas, Austin [Arce, 2002; Galvez, 2004; Okazaki and Engelhardt, 2007; Ryu, 2005], which uses the testing protocol proposed by and Uang [2006] and subsequently adopted by AISC 341-10 [AISC 341-10, 2010] that considers the accumulation of damage in the links for each cycle and compares this to what is typically observed in nonlinear dynamic analysis of

EBF structures using real earthquake ground motion records. Therefore, this loading protocol is more representative of the damage accumulation to EBF links to be expected during an earthquake, which has been noted to have a direct impact on the plastic chord rotation capacity Kuşyilmaz and Topkaya [2015]. Gulec *et al.* [2011] compiles this experimental data and provides a set of limit-state fragility functions for EBF links. These limit-state fragility functions can be integrated into an expression for interstorey drift, such as Equation 10, in the same way the design code prescribed values are. However, by using the values proposed by Gulec *et al.* [2011], the variability of the limit-state values is considered, which is then used in this study for the development of a interstorey drift-based fragility function as opposed to a plastic link rotation-based function. The advantage of using an interstorey drift-based fragility function is that this is more direct when assessing probabilities of exceeding certain limit-states as just the interstorey drift is required, as opposed to the plastic chord rotation demands, which needs to be separated from its elastic components, which can be a tedious task.

3.2.5 EBF Total Interstorey Drift Capacity Expression

In addition to the experimental data from the expression for the plastic drift capacity from Section 3.2.4 together with the yield drift expression from Section 3.2.1, the total drift capacity of a single storey of a short link EBF structure with a single bay and central link element is obtained from the sum of the two as:

$$\theta_{c,i} = \frac{f_y A_{v,i} e_i}{\sqrt{3}(B - e_i)}\left(\frac{e_i(B - e_i)}{12EI_{zz,i}} + \frac{1}{GA_{v,i}}\right) + \frac{2k_{br,i}\varepsilon_y}{\sin(2\alpha_i)} + \frac{2k_{col,i-1}\varepsilon_y H_{i-1}}{B} + \frac{e_i\gamma_p}{B} \qquad \text{Equation 3.10}$$

where the symbols have been defined earlier in Sections 2.1 and 2.4. It should be noted that the above expression is valid for an EBF system with a centrally placed link, as illustrated in Figure 3.1. Should the user require fragility functions for EBF systems with link elements located at one end, the above expressions would need to be revised to consider the different behaviour of such a system. As such, the fragility functions described in this article relate to EBF configurations such as in Figure 3.1, although the same approach could be adopted for other systems.

While it should be clear that this equation could provide a useful indication of the likely drift capacity of an EBF system, it is apparent that not all the data required to use the expression will always be available during the seismic assessment of a building or a group of buildings. For instance, in a regional assessment of the vulnerability of EBF systems one might only have information on the number of storeys and likely material properties of the EBFs. To this extent, the availability of fragility functions that are formulated as a function of various possible input parameters could be quite advantageous. The following sections will illustrate how such fragility functions can be established.

3.3 DEVELOPMENT OF FRAGILITY FUNCTION FOR EBF STRUCTURES

Fragility functions describe the probability of exceeding a predefined damage limit-state given a certain value of EDP. Damage limit-states can be defined at a global level, such as serviceability or collapse, or on a local element level, such as link yielding or fracture. An EDP is a parameter associated with the magnitude of the response of the structure, where typical global EDP's are interstorey drift and floor accelerations and an example of a local EDP is element chord rotation.

3.3.1 Existing EBF Fragility Functions

As previously outlined in Section 2.5, Gulec *et al.* [2011] compiles experimental data from 110 tests documented in the literature to provide a set of damage limit-state fragility functions for EBF links. The damage limit-states are defined in terms of slab damage, link web and flange yielding, and local buckling and fracture observed during the experimental tests, and a set of fragility functions were derived based on these. Such fragility functions have been implemented in PACT [FEMA P58-1, 2012], which is a software tool that performs a seismic performance assessment of structures given the building's dynamic response to earthquakes of ranging return periods. However, one drawback to using the fragility functions proposed in Gulec *et al.* [2011] is that the EDP is specified in terms of plastic link chord rotation (γ_p), as this is typically reported from experimental tests on EBF links. Typically, users input EDPs such as interstorey drift and floor accelerations into PACT for seismic performance assessment. This means that should a fragility function for EBFs be proposed with an EDP in terms of interstorey drift, this would simplify performance assessments as it would remove the need to extract the plastic component of the link element chord rotation demands from the results of structural analyses and would greatly assist loss assessment studies conducted using either a comprehensive approach [FEMA P58-1, 2012; FEMA P58-2, 2012; Porter, 2003] or simplified methods [Porter *et al.*, 2004; Welch *et al.*, 2014], as these types of EDPs are typically used in such loss assessment approaches.

3.3.2 Proposed Approach

In order to derive a set of fragility functions for EBF structures with interstorey drift as the EDP, the expression developed and validated in Section 2 is used in conjunction with distributions for the various parameters affecting storey drift, including to the distributions associated with the different damage limit-state distributions proposed by Gulec *et al.* [2011]. Using the distributions of all of the various parameters, Monte Carlo Simulation (MCS) is used to sample values for each variable and calculate the interstorey drift capacity (θ_c) using Equation 3.10 to give a data set, which describes the distribution of the interstorey drift capacity. Using this distribution of θ_c for a given damage state, a fragility function for an EBF is then derived in terms of interstorey drift, which can be directly used in current seismic performance assessment tools, such as PACT. Section

3.2.3 discussed the sensitivity of θ_y to the various parameters contained within the expression. Four of these; bay width (B), link length (e), number of storeys (n) and link shear area (A_v), are variables that heavily influence θ_c but are considered deterministic variables, as opposed to probabilistic variables with an associated distribution. As such, fragility functions are developed in terms of a specific combination of bay width, link length, storey number, link section and damage limit-state. It is important to acknowledge the sources of uncertainty that exist within the fragility functions developed using the proposed approach. Firstly, the aleatory uncertainty in the drift capacity is introduced via the dispersion in the test data reported by Gulec *et al.* [2011], since this dispersion represents the randomness in the drift capacity of EBF links seen in experimental testing. Secondly, an additional uncertainty known as epistemic uncertainty is introduced in the proposed approach as this reflects the uncertainty in knowing the actual drift capacity. However, for the various sets of fragility function sets discussed in Section 3.4, it will be shown that with increased knowledge of the EBF structure, the epistemic uncertainty can be reduced.

3.3.3   Probabilistic and Deterministic Distributions of Yield Drift Parameters

As discussed in Section 3.2, some of the variables used in the MCS of Equation 3.10 are assigned a distribution and some are assigned deterministic values. The values for storey height (h), elastic (E) and shear (G) moduli of steel are taken here to be 3.5m, 210GPa and 81GPa, respectively. These are kept constant throughout the analysis, as Equation 3.10 has been shown to be relatively insensitive to these terms. As for deterministic values, the link size and length, bay length and number of storeys are all deterministic values envisaged as known parameters by the user and are variables that do not constitute a distribution, but rather a predetermined range of values. This was conducted for EBF systems with a number of storeys between 1 and 15 and the entire European HEA, HEB and HEM section size catalogue [Corus, 2006]. Since short links are defined by a ratio ρ less than 1.6, which is a function of the link cross-section and link length, the maximum possible link length can be determined for a given section in order for it to still be classified as a short link by rearranging Equation 3.1. Therefore for each section, the maximum link length (e_{max}) in order to be still classified as a short link according to a rearranged Equation 3.1 was determined for each cross-section and four link lengths equal to 40%, 60%, 80% and 100% of e_{max} were used in the simulations. Bay widths were varied between 5 and 12m in increments of 1m.

Values for the yield strength of steel (f_y), link plastic chord rotation capacity (γ_p), brace axial load ratio (k_{br}) and average column axial load ratio (k_{col}) are all taken to be probabilistic values with an associated mean and dispersion. These values are listed in Table 2 along with the other values and their associated distributions. For the steel yield strength, experimental testing by Braconi *et al.* [2010] on European grade S355 steel is

taken as the distribution for f_y, which is a normal distribution with a mean of 355MPa and standard deviation of 27MPa. For the axial load ratios of the braces (k_{br}) and columns (k_{col}), a series of pushovers of a total of 38 EBF structures presented in Rossi and Lombardo [2007] and O'Reilly and Sullivan [2015] has provided a set of values for buildings designed in that report, which allows a reasonable value of median and standard deviation to be estimated in both cases. Since a normal distribution is assumed for both the k_{br} and k_{col}, any samples that give values outside the range of 0 and 1 are removed from the simulation, as these do not represent physically possible scenarios.

The distributions of link plastic chord rotation capacity come from the data published by Gulec *et al.* [2011] for three limit-states identified from the test results and engineering judgement. These three damage limit-states corresponded to:

- Damage State 1 (DS1): plastic chord rotation resulting in concrete slab repair being required.
- Damage State 2 (DS2): plastic chord rotation for which heat straightening of the link is required.
- Damage State 3 (DS3): plastic chord rotation resulting in complete link replacement being required.

These values are given as lognormal distributions by Gulec *et al.* [2011] and their associated values are given in Table 2. The link stiffener spacing considered was such that the links used in the dataset satisfied the AISC 341-10 maximum link stiffener spacing of $30t_w$-d/5, where t_w is the web thickness of the link section and d is the depth of the section. In addition, some uncertainty associated with the data presented in Gulec *et al.* [2011] arises from the effects of loading protocol on the link capacity, where depending on the loading history to test the link member, different plastic rotation capacities can be observed. This was highlighted by Richards and Uang [2006] where it was concluded that the loading protocol used by researchers at the University of California, Berkeley such as Engelhardt and Popov [1989a] was too severe and the actual plastic chord rotation capacity ought to be a little higher than reported from those tests if a different loading protocol was used. Further testing by Okazaki *et al.* [2009] at the University of Texas using a revised loading protocol for short links showed a slightly larger plastic chord rotation capacity of the links. Data from both tests has been included in the dataset used in Gulec *et al.* [2011] and no distinction is made between different loading protocols, which is acknowledged here as a source of uncertainty.

Table 3.2: Random variable distribution models and associated values.

Parameter		Unit	Distribution Model	Median	Dispersion
Link length	e	m	Deterministic	-	-
Number of storeys	n	-	Deterministic	-	-
Link shear area	A_v	mm^2	Deterministic	-	-
Bay width	B	m	Deterministic	-	-
Yield strength	f_y	MPa	Normal	355	27
Brace axial load ratio	k_{br}	-	Normal	0.3	0.1
Column axial load ratio	k_{col}	-	Normal	0.4	0.1
Link plastic chord rotation	γ_p (DS1)	rad	Lognormal	0.040	0.30
Link plastic chord rotation	γ_p (DS2)	rad	Lognormal	0.056	0.30
Link plastic chord rotation	γ_p (DS3)	rad	Lognormal	0.076	0.34

3.3.4 Analysis and Results

The MCS of the parameters outlined in Table 3.2 using Equation 3.10 yielded over 5000 simulations, where 1000 values were sampled for each of the random variables listed in Table 3.2. Each of these simulations were tested using the Lilliefors goodness-of-fit test at the 5% significance level [Ang and Tang, 2007], which were tested against the null hypothesis that the interstorey drift capacity was of a lognormal distribution. Each simulation returned the result that the null hypothesis could not be rejected at the 5% significance level. An example of the results of such a simulation is shown in Figure 3.8, where the simulated data is shown alongside its fitted lognormal distribution. The plot of observed distribution of the interstorey drift capacity data from the MCS versus that predicted by the fitted distribution shows a one-to-one plot of the comparison between the data's cumulative distribution function and the fitted lognormal distribution. The simulated data from the MCS was fitted to a lognormal using the method of moments [Ang and Tang, 2007], where the median and dispersion for the simulated data was fitted to the corresponding lognormal distribution given the Lilliefors test acceptance.
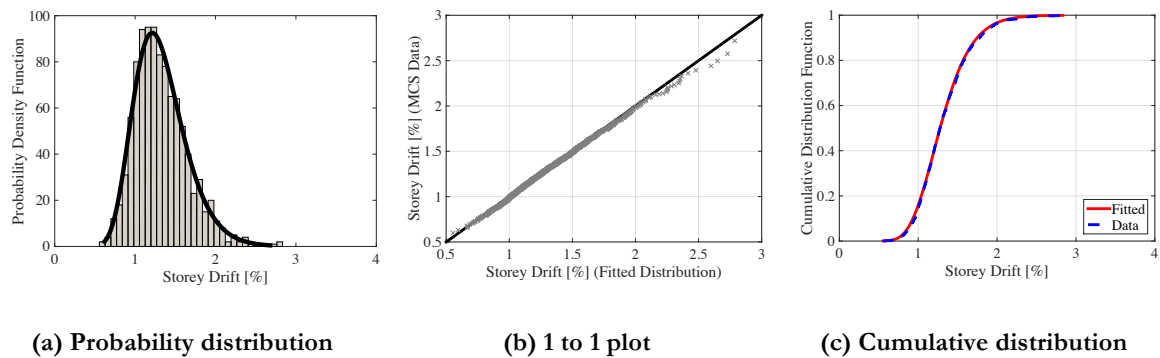

(a) Probability distribution   (b) 1 to 1 plot   (c) Cumulative distribution

Figure 3.8: Simulation results example (HE260B, n=5, e=0.781m, B=7m, DS3).

3.4 PROPOSED FRAGILITY FUNCTION FOR EBF STRUCTURES

3.4.1 Overview

For each of the damage limit-states, the individual cumulative distribution functions (CDF's) for each simulation are reported in the following three ways:

1. Generic EBF Fragility: The fragility functions for each of the damage limit-states are reported that do not need specification of any details, and are hence termed the general fragility function set. This set considers all of the different link section sizes, link lengths, bay widths and storey numbers simulated in the dataset and hence the dispersion associated with this fragility function set is relatively large as a result. Since this is a more global fragility curve set, it can be used to assess the performance of the EBF structures on a more regional scale without actually knowing many details about the structures.

2. Storey Specific EBF Fragility: A storey specific set of fragility functions is presented, where the storey number being considered within a structure is specified to reduce the dispersion in the general fragility set. This specification of terms could be equally done for link length or section size, but given the rigid body rotation's prominence in yield drift contribution to higher storey buildings shown in Figure 3.4, a refinement in terms of the storey number only was carried out also considering that the storey number is an easy parameter to determine in building assessment.

3. Refined EBF Fragility: Since the MCS performed to generate these fragility function sets was performed using Equation 3.10 with the relevant distributions of the variables outlined in Table 2, it is proposed that this expression can be used directly to determine a median drift by just specifying the median values of the input parameters for a given case. The dispersion associated with this median could then be approximated based off of the observed dispersion of the MCS results. This approach has the advantage of giving the user more control for the specification of parameters, while simplifying the probabilistic side through the adoption of a reasonable dispersion based on the results of more thorough analysis.

Lastly, the code used to perform the MCS of the data is converted into a MATLAB [MATLAB, 2014] based function, where the user can specify the details of the building directly and receive a set of fragility functions for that specific case through the MCS method outlined above. These four approaches are then compared for an example storey in a structure to demonstrate their applicability and how they can be used to perform a quick general assessment or a more detailed assessment, depending on the level of detail known about an EBF structure.

3.4.2 Generic EBF Fragility Function

Should a general set of fragility functions irrespective of link section size, link length, bay width and number of storeys be required for general or regional assessment, Table 3.3 shows the values for the three limit-states considered, where Figure 3.9 shows the plot of these fragility functions along with the individual fragility functions used to generate them from each MCS and are plotted together in Figure 3.10.

Table 3.3: Mean and dispersion for a general fragility function.

|	$\hat{\theta}$ [%]	β
DS1	1.04	0.48
DS2	1.23	0.48
DS3	1.48	0.49

As can be seen from Figure 3.9, the range of the fragility functions is quite wide although for individual curves, the dispersion is quite low but the general combined function is quite disperse reflecting the wide range of fragility functions for each MCS considered.

### 3.4.3 Storey Specific EBF Fragility Function

Should the storey number (i) within a structure be known, the fragility function set shown in Figure 3.10 can be refined further, which will reduce the associated dispersion for these damage limit-states. Table 3.4 shows the median and dispersion for up to fifteen storeys, which were considered in the analysis for each limit-state. As such, if one were interested in the fragility at DS3 of the 4th floor of an EBF structure, possessing a total number of storeys anywhere between 4 and 15 storeys, then from Table 3.4 they would estimate the median drift capacity of 1.38% and a dispersion of 0.42. As expected, the median drift increases between damage limit-state and also with increasing height due to the increase in the contribution of the rigid body rotation as a result of the axial shortening of the columns in the lower storeys. It is also noticed that the dispersion of the values is greatly decreased with respect to the general set shown in Table 3.3 and Figure 3.10, where the storey number was not specified. This highlights how the dispersion of the fragility function sets can be reduced should more details be known about the structure. It is also worth noting that the dispersion associated with the data decreases as one increases the storey number of the structure. That is, if the fragility function set of the first level of a structure is compared to what would be used for the fifteenth level of the structure; the dispersion is much less at the fifteenth level's than at the first. This is because as the storey number increases, so too does the contribution of the rigid body rotation of the lower storeys to the interstorey drift capacity, as was seen in Figure 3.4. The main variables associated with this contribution are the terms k_{col} and f_y, and the corresponding

standard deviation's of these terms are quite low in comparison to others in Equation 3.10, thus providing reason that as this term with a relatively low dispersion becomes more prominent, the overall dispersion is to decrease.
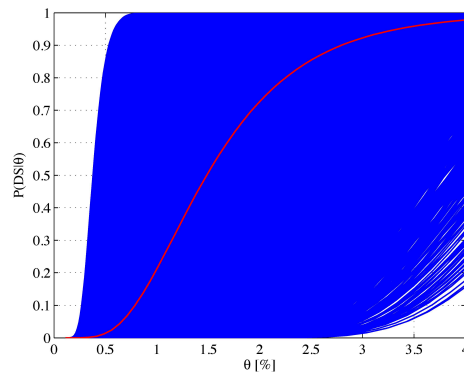
(a) DS1
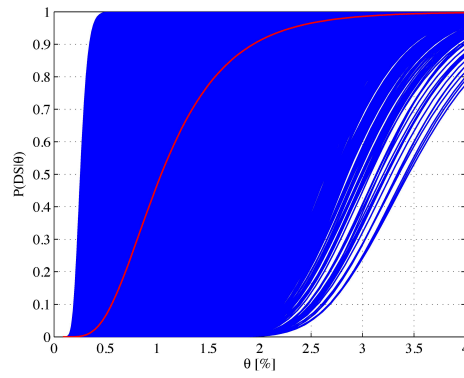
(b) DS2
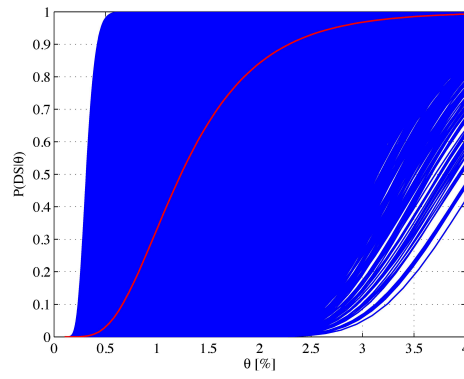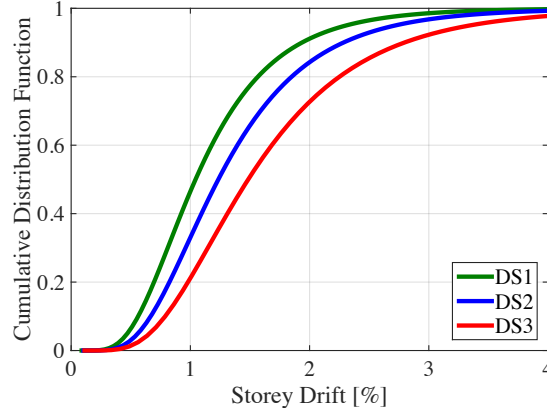

(c) DS3

Figure 3.9: General EBF fragility functions.

Figure 3.10: Proposed EBF fragility functions.

Table 3.4: Median and dispersion for a storey-based fragility function.

i	DS1		DS2		DS3	
	$\hat{\theta}$ [%]	β	$\hat{\theta}$ [%]	β	$\hat{\theta}$ [%]	β
1	0.68	0.44	0.89	0.46	1.17	0.49
2	0.75	0.40	0.96	0.42	1.24	0.46
3	0.81	0.37	1.03	0.39	1.31	0.44
4	0.88	0.34	1.10	0.37	1.38	0.42
5	0.95	0.32	1.16	0.36	1.44	0.40
6	1.02	0.31	1.23	0.34	1.51	0.38
7	1.08	0.30	1.30	0.33	1.58	0.37
8	1.15	0.29	1.37	0.32	1.65	0.36
9	1.22	0.28	1.43	0.31	1.72	0.35
10	1.29	0.27	1.50	0.30	1.78	0.34
11	1.35	0.27	1.57	0.29	1.85	0.33
12	1.42	0.26	1.64	0.28	1.92	0.32
13	1.49	0.26	1.70	0.28	1.99	0.31
14	1.56	0.25	1.77	0.27	2.05	0.31
15	1.62	0.25	1.84	0.27	2.12	0.30

3.4.4 Refined EBF Fragility Function

As mentioned previously, it is also proposed to use the drift capacity relationship outlined in Equation 3.10 for the direct calculation of a median interstorey drift capacity, followed by an assumption for the associated dispersion. This allows for the direct calculation of median interstorey drift values using the information regarding link dimensions, storey number and bay width. Equation 3.10 is rewritten in a more simplified form with the

inclusion of some terms in Table 3.2 to allow easier use when inputting the basic variables required. This way only the link dimensions (A_v, e, I_{zz}), storey number within the structure (i), steel grade (f_y, E, G), bay length (B) and are required to give the median value of drift capacity for a given damage limit-state ($\gamma_p(DS)$):

$$\hat{\theta}_{c,i} = \frac{f_y A_{v,i} e_i}{\sqrt{3}(B-e_i)}\left(\frac{e_i(B-e_i)}{12EI_{zz,i}} + \frac{1}{GA_{v,i}}\right) + \frac{0.6f_y}{E\sin\left(2\arctan\dfrac{2h_i}{B-e_i}\right)} + \frac{0.6f_y h_i(i-1)}{BE} + \frac{e_i\gamma_p(DS)}{B}$$ **Equation 3.11**

Using this in conjunction with an assumed dispersion based on results of the MCS, a set of fragility functions can be formed rather easily. Appropriate values to be assumed for this dispersion are found from examination of the values observed from the Monte Carlo Simulation for each damage state. Collecting the dispersion values for each of the damage states, Figure 3.11 shows the corresponding dispersion versus median drift capacity for each of the damage states. From this, there is a trend in the increase of the dispersion values between damage states. Using Figure 3.11 as an indication of appropriate values for the anticipated dispersion values to be used in conjunction with Equation 3.11, the average values shown in Figure 3.11 are proposed here.

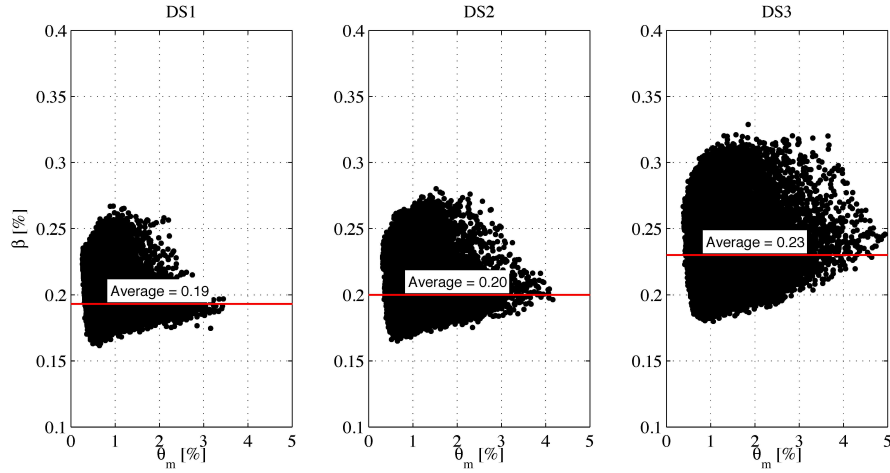**Figure 3.11: Observed β from the Monte Carlo Simulation of each damage state.**

3.4.5   MATLAB Tool for Specific Case Fragility Function Generation

In addition to the storey based and general fragility functions outlined above, a MATLAB function is available which allows users to generate their own set of fragility functions for a given combination of link section, length and storey number. This tool functions by

performing the MCS approach used in this study, but allows users to specify an exact combination of the three deterministic values, as opposed to general values such as those specified in Table 3.3 and Table 3.4. The function performs the Lilliefors goodness-of-fit test to the simulated data as before and reports a set of median and dispersion values for each of the damage limit-states considered. In addition, should the user want to refine their interstorey drift-based fragility function set for a specific EBF structure, the MATLAB based tool provided allows for the user to specify all of the relevant parameters such as bay width, storey height, steel yield strength etc. in conjunction with the existing plastic chord rotation-based functions to result in an interstorey drift-based set of functions that have been directly converted to interstorey drift-based functions, given the users inputs. This essentially means that the user has converted the fragility functions from a plastic chord rotation-based set to interstorey drift-based set instead of converting the interstorey drifts demands to plastic chord rotation demands to be input into PACT, which would create an additional EDP to track within the program. Further information and guidelines on how to implement the function are found at https://www.dropbox.com/s/ejkk5amr6r727ey/EBF_fragility.zip?dl=0.

3.4.6 Example Fragility Function Generation for a 5 Storey EBF

An example case study is examined to demonstrate the use of each of the four methods of establishing fragility function sets, depending on the availability of information and the required level of accuracy of the results. The example structure is to be taken as the fifth storey in a 10 storey EBF structure consisting of a HE220B link section with 600mm length and 7m bay width. Firstly, for the general set of functions presented in Section 3.4.2, these medians and dispersions are taken directly for the case study and reported in Table 3.5.

Table 3.5: Case study fragility curves.

Method	DS1		DS2		DS3	
	θ_c %	β	θ_c %	β	θ_c %	β
Generic	1.04	0.48	1.23	0.48	1.48	0.49
Storey Specific	0.95	0.32	1.16	0.35	1.44	0.40
Refined	0.71	0.19	0.84	0.20	1.01	0.23
MATLAB	0.75	0.18	0.89	0.20	1.05	0.23

For the storey number based set in Section 3.4.3, the set of functions corresponding to an i of 5 in Table 3.4 are selected. For the calculation of the median using Equation 3.11, the median values of the required variables are used and the median values are reported in Table 3.5. For the dispersion values of each of these damage states, the values reported in Figure 3.11 are adopted. For the MATLAB function method, the required input is used

and the results included also in Table 3.5. A plot of each of these fragility function sets is presented in Figure 3.12 for each damage state. As can be seen, there is some degree of variability between the fragility function sets, depending on the level of detail input to obtain them where the more general fragility functions from Section 3.4.2 and 3.4.3 gave higher median interstorey drift and dispersion compared with the other two approaches in this case. Since the MATLAB function performs a MCS of the known scenario, this is taken to be the actual fragility function based on the results of this study. Figure 3.12 shows that the calculation of median drift capacities through Equation 3.11, and subsequently taking an assumed value of dispersion based on simulated data results, gave quite good results when compared with the result of the MATLAB function's exact scenario simulation.
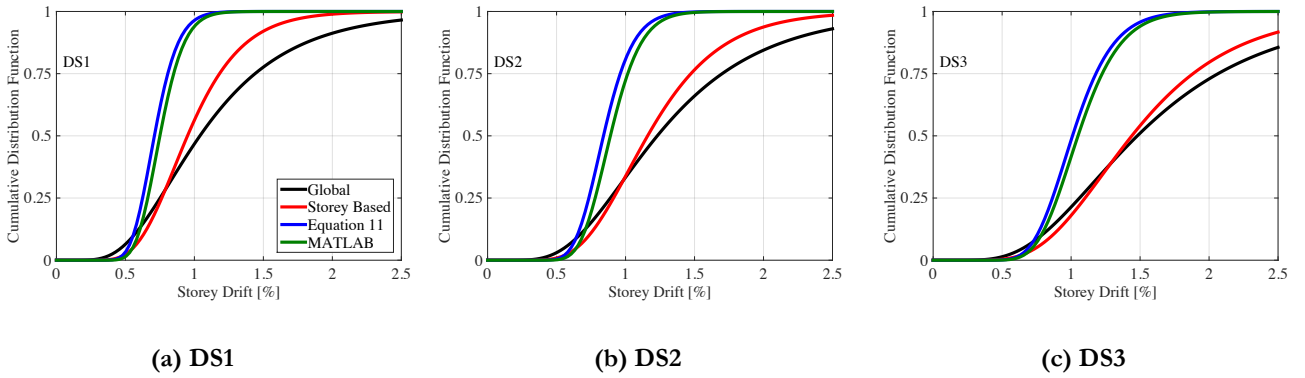

(a) DS1   **(b) DS2**   **(c) DS3**

Figure 3.12: Case study fragility functions.

For cases when multi-bay EBF structures are being assessed with different bay lengths and link details, numerous sets of fragility functions will result, where the probability of each damage state will be computed for each bay using the bay's associated fragility function set for a given interstorey drift demand at a each floor. This applies to the case of the refined EBF fragility function outlined in Section 3.4.4 and the MATLAB based approach in Section 3.4.5. For the approaches outlined in Sections 3.4.2 and 3.4.3, the variability of bay length and link size has been accounted for through the epistemic uncertainty introduced during the Monte Carlo Simulation of the fragility functions, hence these general fragility function sets are valid for different bay lengths and link sizes. However, it is again highlighted that the fragility function sets developed in this article apply to EBFs with link elements placed in the centre of the bay, as illustrated in Figure 3.1.

3.5 SUMMARY

The derivation of an interstorey drift-based fragility function set for EBF structures has been discussed. Analytical expressions for the determination of the yield drift of a given EBF configuration were reviewed and subsequently validated by comparing the results obtained from Equation 3.8 to those given by a series of pushovers of EBFs using an experimentally calibrated numerical model. Using the yield drift expression, a sensitivity study was conducted to determine the parameters most affecting the yield drift and ultimately, the drift capacity of an EBF system. This led to the determination of a set of parameters, which were identified to heavily influence the drift capacity of an EBF. A Monte Carlo Simulation (MCS) of this expression was conducted using a set of deterministic values and probabilistic distributions for the various influential variables. The resulting simulation led to the development of storey number based fragility function set, considering various link damage limit-states, a generic fragility function which does not require any knowledge of the EBF details, a storey-specific fragility function which is dependant only on the storey number, and a refined fragility function that is obtained using an expression to analytically derive median values to be used along with assumed values of dispersion. Lastly, a MATLAB code for specific fragility function set generation using the MCS process outlined to generate the previous two general sets is provided to allow computation of scenario specific fragility functions, should the user require such a level of refinement.

4. CONCLUSIONS

4.1 SUMMARY AND CONCLUSIONS

As a result of the research presented in Chapter 2 regarding the direct displacement-based seismic design of EBF structures, the following concluding remarks can be made:

- There appear to be shortcomings with the current Eurocode 8 method in terms of accurately controlling link member deformation demands. In addition, it has been demonstrated that unique force reduction (behaviour) and displacement amplification factors are not applicable to all types of EBF configurations as the system ductility capacity varies as a function of geometrical and material properties.
- Some discrepancy exists in the computation of design plastic link demands using Eurocode 8 with inadequate account for the localised concentration of deformation demands in the link elements when EBF move into the inelastic range of response. Results obtained using a newly proposed adjustment factor compared well with pushover results and thus the adjustment is recommended for incorporation into Eurocode 8, noting that the US provisions already consider this issue in design.
- A numerical model that captures the behaviour of short link elements was proposed, and the results of experimental tests were used to validate the parameters and thus propose relatively simple numerical modelling guidelines for EBF systems that represent the isotropic hardening and hysteretic behaviour quite well.
- A spectral displacement reduction factor expression has been developed for EBFs using a newly calibrated hysteretic model for the link members. Information on the dispersion associated with the DRF expression was also provided.
- For each of the case study structures designed, nonlinear time-history analyses using a set of spectrum compatible ground motions and an experimentally validated numerical modelling approach demonstrated the satisfactory performance of each of the case study structures, thus demonstrating the robustness of the DDBD method for the seismic design of EBF structures.
- Existing amplification factors for the estimation of capacity design actions on columns and braces in EBFs have been found to provide adequate protection of these non-dissipative zones during seismic response.

As a result of the research presented in Chapter 3 regarding the development of a fragility functions for the damage assessment of EBF structures, the following concluding remarks can be made:

- An interstorey drift-based fragility function has been established for EBFs, which identifies three different link damage limit-states reported from experimental testing. This leads to a more direct assessment of damage, and subsequently losses, for an EBF structure when carrying out a probabilistic loss assessment of an EBF structure.
- Should more detailed information be available regarding the EBF structure, a set of fragility functions can be established by first determining the median values for each damage state, followed by an assumption of the associated dispersion based on previous MCS results. A case study example demonstrated that this approach was the most accurate at determining the median values of interstorey drift capacity when compared with MCS results in addition to having a reduced dispersion compared to the more general fragility function sets.
- A MATLAB based fragility function tool has been developed that allows users to generate a more refined set of fragility functions corresponding to the damage limit-states outlined in Section 4 by performing a Monte Carlo Simulation of the user defined parameters for the EBF. This essentially means that the user has converted the fragility functions from a plastic chord rotation-based set to interstorey drift-based set instead of converting the interstorey drifts demands to plastic chord rotation demands.
- In addition to providing a set of fragility functions that can be used for performance assessment, these fragility functions can be used to determine the likelihood that a given link in an EBF structure has exceeded a certain damage state and requires repair. This could be particularly useful when considering the observations of Clifton *et al.* [2011] during reconnaissance inspections of EBF structures following the 2010 and 2011 Canterbury earthquakes in New Zealand, where it was reported that architectural and floor finishes inhibited proper inspection of the links following the event. However, a set of fragility functions such as those developed in this paper could be used to determine the likelihood of damage and justify the need for intervention and full structural inspection should information on the maximum interstorey drift be available.

REFERENCES

AISC 341-05. [2005] *Seismic Provisions for Structural Steel Buildings*, Chicago, IL, USA.

AISC 341-10. [2010] *Seismic Provisions for Structural Steel Buildings*, Chicago, IL, USA.

AISC 360-10. [2010] *Specification for Structural Steel Buildings*, Chicago, IL, USA.

Ang, A., Tang, W. [2007] *Probability Concepts in Engineering, Emphasis on Applications in Civil and Environmental Engineering*, John Wiley & Sons, Ltd.

Arce, G. [2002] "Impact of higher strength steels on local buckling and overstrength of links in eccentrically braced frames," The University of Texas at Austin.

ASCE 7-10. [2010] *Minimum Design Loads for Buildings and Other Structures*, Reston, VA, USA.

Badalassi, M., Braconi, A., Caprili, S., Salvatore, W. [2011] "Seismic structural performance of EBF - influence of steel yielding stress limitations on collapse modes.," *EUROSTEEL 2011*.

Braconi, A., Badalassi, M., Salvatore, W. [2010] "Modeling of European steel qualities mechanical properties scattering and its influence on Eurocode 8 design requirements," *14ECEE - European Conference on Earthquake Engineering*, Ohrid, Macedonia.

Bruneau, M., Anagnostopoulou, M., MacRae, G. A., Clifton, C., Fussell, A. [2010] "Preliminary Report on Steel Building Damage from the Darfield Earthquake of September 4, 2010," *Bulletin of the New Zealand Society for Earthquake Engineering*, Vol. 43, No.4, pp. 351–359.

Bruneau, M., Clifton, C., MacRae, G. A., Leon, R., Fussell, A. [2011] "Steel Building Damage from the Christchurch Earthquake of February 22, 2011," *Bulletin of the New Zealand Society for Earthquake Engineering*, Vol. Draft.

Chopra, A. K. [2012] *Dynamics of Structures: Theory and Applications to Earthquake Engineering*, Prentice Hall, Englewood Cliffs, New Jersey.

Clifton, C., Bruneau, M., MacRae, G. A., Leon, R., Fussell, A. [2011] "Steel Structures Damage from the Christchurch Earthquake Series of 2010 and 2011," *Bulletin of the New Zealand Society for Earthquake Engineering*, Vol. 44, No.4, pp. 297–318.

Della Corte, G., D'Aniello, M., Landolfo, R. [2013] "Analytical and numerical study of plastic overstrength of shear links," *Journal of Constructional Steel Research*, Vol. 82, pp. 19–32.

Corus. [2006] *Structural Sections to BS4: Part 1: 1993 and BS EN10056: 1999*, North Lincolnshire, U.K.

CSA S16-09. [2009] *Design Of Steel Structures*, Ontario, Canada.

Dwairi, H. M., Kowalsky, M. J., Nau, J. M. [2007] "Equivalent Damping in Support of Direct Displacement-Based Design," *Journal of Earthquake Engineering*, Vol. 11, No.4, pp. 512–530.

EN 1993-1-1:2005. [2005] *Eurocode 3: Design of Steel Structures - Part 1-1: General Rules and Rules for Buildings*, Brussels, Belgium.

EN 1998-1:2004. [2004] *Eurocode 8: Design of Structures for Earthquake Resistance - Part 1: General Rules, Seismic Actions and Rules for Buildings*, Brussels, Belgium.

Engelhardt, M. D., Popov, E. P. [1989a] *Behavior of Long Links in Eccentrically Braced Frames*, Berkeley, California.

Engelhardt, M. D., Popov, E. P. [1989b] "On Design of Eccentrically Braced Frames," *Earthquake Spectra*, Vol. 5, No.3, pp. 495–511.

Faccioli, E., Paolucci, R., Rey, J. [2004] "Displacement Spectra for Long Periods," *Earthquake Spectra*, Earthquake Engineering Research Institute, Vol. 20, No.2, pp. 347–376.

FEMA P58-1. [2012] *Seismic Performance Assessment of Buildings: Volume 1 - Methodology (P-58-1)*, Washington, DC.

FEMA P58-2. [2012] *Seismic Performance Assessment of Buildings: Volume 2 - Implementation Guide (P-58-2)*, Washington, DC.

Galvez, P. [2004] "Investigation of factors affecting web fractures in shear links," The University of Texas at Austin.

Goel, S. C., Liao, W. C., Reza Bayat, M., Chao, S. H. [2009] "Performance-based plastic design (PBPD) method for earthquake-resistant structures: an overview," *The Structural Design of Tall and Special Buildings*, Vol. 19, No.1-2, pp. 115–137.

Grant, D., Blandon, C. A., Priestley, M. J. N. [2005] *Modelling inelastic response in direct displacement based design*, Pavia, Italy.

Gulec, C. K., Gibbons, B., Chen, A., Whittaker, A. S. [2011] "Damage states and fragility functions

for link beams in eccentrically braced frames," *Journal of Constructional Steel Research*, Elsevier Ltd, Vol. 67, No.9, pp. 1299–1309.

Gulkan, P., Sozen, M. A. [1974] "Inelastic Responses of Reinforced Concrete Structures to Earthquake Motions," *ACI Journal*, Vol. 71, No.12, pp. 604–610.

Hjelmstad, K., Popov, E. P. [1983] *Seismic Behavior of Active Beam Links in Eccentrically Braced Frames*, Berkeley, California.

Jacobsen, L. S. [1930] "Steady forced vibration as influencd by damping," *Transactions of ASME*, Vol. 52, No.15, pp. 169–181.

Kanvinde, A. M., Marshall, K. S., Grilli, D. A., Bomba, G. [2014] "Forensic Analysis of Link Fractures in Eccentrically Braced Frames during the February 2011 Christchurch Earthquake : Testing and Simulation," *Journal of Structural Engineering*, Vol. 141, No.5.

Kasai, K., Popov, E. P. [1986] *A Study of Seismically Resistant Eccentrically Braced Steel Frame Systems*, Berkeley, California.

Kuşyilmaz, A., Topkaya, C. [2015] "Displacement amplification factors for steel eccentrically braced frames," *Earthquake Engineering & Structural Dynamics*, Vol. 44, No.2, pp. 167–184.

Malakoutian, M., Berman, J. W., Dusicka, P. [2013] "Seismic response evaluation of the linked column frame system," *Earthquake Engineering & Structural Dynamics*, Vol. 42, No.September 2012, pp. 795–814.

Maley, T. J., Sullivan, T. J., Lago, A., Roldan, R., Calvi, G. M. [2013] *Characterising the Seismic Behaviour of Steel MRF Structures*, EUCENTRE Report 2013/02. Pavia, Italy.

Mansour, N. [2010] "Development of the Design of Eccentrically Braced Frames with Replaceable Shear Links," University of Toronto.

MATLAB. [2014] *Version 8.3.0 (R2014a)*, The Mathworks Inc., Natick, Massachusetts.

Mazzolani, F. M., Landolfo, R., Della Corte, G., Faggiano, B. [2006] *Edifici con Struttura di Acciaio in Zona Sismica*, Pavia, Italy.

McKenna, F., Fenves, G., Filippou, F. C., Mazzoni, S. [2000] "Open System for Earthquake Engineering Simulation (OpenSees)," <http://opensees.berkeley.edu/wiki/index.php/Main_Page>.

Mohebkhah, A., Chegeni, B. [2014] "Overstrength and rotation capacity for EBF links made of European IPE sections," *Thin-Walled Structures*, Vol. 74, pp. 255–260.

Nascimbene, R., Rassati, G. A., Wijesundara, K. K. [2012] "Numerical Simulation of Gusset Plate Connections with Rectangular Hollow Section Shape Brace Under Quasi-Static Cyclic Loading," *Journal of Constructional Steel Research*, Vol. 70, pp. 177–189.

Nievas, C. I., Sullivan, T. J. [2015] "Applicability of the direct displacement-based design method to steel moment resisting frames with setbacks," *Bulletin of Earthquake Engineering*.

NZS 3404. [2007] *Steel Structures Standard*, Wellington, New Zealand.

O'Reilly, G. J., Sullivan, T. J. [2015] "Direct Displacement-Based Seismic Design of Eccentrically Braced Steel Frames," *Journal of Earthquake Engineering*, Taylor & Francis, pp. 1–36.

O'Reilly, G. J., Sullivan, T. J. [2016] "Fragility Function for Eccentrically Braced Frame Structures," *Earthquakes and Structures*, Vol. XX, No.(Accepted).

Okazaki, T., Arce, G., Ryu, H. C., Engelhardt, M. D. [2005] "Experimental Study of Local Buckling, Overstrength, and Fracture of Links in Eccentrically Braced Frames," *Journal of Structural Engineering*, American Society of Civil Engineers, Vol. 131, No.10, pp. 1526–1535.

Okazaki, T., Engelhardt, M. D. [2007] "Cyclic loading behavior of EBF links constructed of ASTM A992 steel," *Journal of Constructional Steel Research*, Vol. 63, No.6, pp. 751–765.

Okazaki, T., Engelhardt, M. D., Drolias, A., Schell, E., Hong, J. K., Uang, C. M. [2009] "Experimental investigation of link-to-column connections in eccentrically braced frames," *Journal of Constructional Steel Research*, Vol. 65, No.7, pp. 1401–1412.

Pennucci, D., Sullivan, T. J., Calvi, G. M. [2011] "Displacement Reduction Factors for the Design of Medium and Long Period Structures," *Journal of Earthquake Engineering*, Vol. 15, No.sup1, pp. 1–29.

Popov, E. P., Kasai, K., Engelhardt, M. D. [1987] "Advances in Design of Eccentrically Braced Frames," *Earthquake Spectra*, Vol. 3, No.1, pp. 43–55.

Popov, E. P., Malley, J. O. [1983] *Design of Links and Beam-To-Column Connections for Eccentrically Braced Steel Frames*, Berkeley, California.

Porter, K. A. [2003] "An Overview of PEER's Performance-Based Earthquake Engineering Methodology," *Proceedings of Ninth International Conference on Applications of Probability and Statistics in Engineering*, San Francisco, CA.

Porter, K. A., Beck, J. L., Shaikhutdinov, R. V. [2004] "Simplified Estimation of Economic Seismic Risk for Buildings," *Earthquake Spectra*, Vol. 20, No.4, pp. 1239–1263.

Priestley, M. J. N. [1993] "Myths and Fallacies in Earthquake Engineering- Conflicts between design and reality," *Bulletin of the New Zealand Society for Earthquake Engineering*, Vol. 26, No.3, pp. 329–341.

Priestley, M. J. N., Calvi, G. M., Kowalsky, M. J. [2007] *Displacement Based Seismic Design of Structures*, IUSS Press, Pavia, Italy.

Richards, P. W., Uang, C. M. [2006] "Testing Protocol for Short Links in Eccentrically Braced Frames," *Journal of Structural Engineering*, American Society of Civil Engineers, Vol. 132, No.8, pp. 1183–1191.

Roeder, C. W., Popov, E. P. [1977] *Inelastic Behavior of Eccentrically Braced Steel Frames Under Cyclic Loadings*, Berkeley, California.

Roldan, R., Welch, D. P., Nievas, C. I., Sullivan, T. J., Calvi, G. M. [2014] *Guidelines for the Performance-Based Seismic design of Steel MRF Structures*, Pavia, Italy.

Rossi, P. P., Lombardo, A. [2007] "Influence of the link overstrength factor on the seismic behaviour of eccentrically braced frames," *Journal of Constructional Steel Research*, Vol. 63, No.11, pp. 1529–1545.

Ryu, H. C. [2005] "Effects of loading history on the behavior of links in seismic-resistant eccentrically braced frames," The University of Texas at Austin.

Shibata, A., Sozen, M. A. [1976] "Substitute-Structure Method for Seismic Design in R/C," *Journal of the Structural Division*, ASCE, Vol. 102, No.1, pp. 1–18.

Sullivan, T. J. [2011] "An Energy-Factor Method for the Displacement-Based Seismic Design of RC Wall Structures," *Journal of Earthquake Engineering*, Vol. 15, No.7, pp. 1083–1116.

Sullivan, T. J. [2013a] "Highlighting Differences Between Force-Based and Displacement-Based Design Solutions for RC Frame Structures," *Structural Engineering International*, No.2, pp. 112–131.

Sullivan, T. J. [2013b] "Direct displacement-based seismic design of steel eccentrically braced frame structures," *Bulletin of Earthquake Engineering*, Vol. 11, No.6, pp. 2197–2231.

Sullivan, T. J., Priestley, M. J. N., Calvi, G. M. (Eds.). [2012] *A Model Code for the Displacement-Based Seismic Design of Structures - DBD12*, IUSS Press, Pavia, Italy.

Sullivan, T. J., Welch, D. P., Calvi, G. M. [2014] "Simplified seismic performance assessment and implications for seismic design," *Earthquake Engineering and Engineering Vibration*, Vol. 13, No.Supp1, pp. 95–122.

Tanabashi, R., Kaneta, K., Ishida, T. [1974] "On the rigidity and ductility of steel bracing assemblages," *5th World Conference on Earthquake Engineering*, Rome, Italy.

Uriz, P., Mahin, S. A. [2008] *Toward Earthquake-Resistant Design of Concentrically Braced Steel-Frame Structures*, Berkeley, California.

Welch, D. P., Sullivan, T. J., Calvi, G. M. [2014] "Developing Direct Displacement-Based Procedures for Simplified Loss Assessment in Performance-Based Earthquake Engineering," *Journal of Earthquake Engineering*, Vol. 18, No.2, pp. 290–322.

Whittaker, A. S., Uang, C. M., Bertero, V. V. [1987] *Earthquake Simulation Tests and Associated Studies of a 0.3 Scale Model of a Six-Story Eccentrically Braced Steel Structure*, Berkeley, California.